The use of thermoluminescent dosimeters for In-vivo dosimetry in a fast neutron therapy beam.

Khumbulani John Bhengu

Thesis presented in fulfilment of the degree of Master of Science in Medicine (Medical Physics) at the University of Cape Town.

March 2000

Supervisors: Dr D.T.L. Jones

Dr K.M. Langen

Acknowledgements

I would like to express my sincere gratitude to the following for making this thesis possible:

- My supervisors, Dr Dan Jones for his patient guidance and support throughout the project, and a special thanks to Dr Katja Langen for her continued encouragement, her interest in the work and assistance in the preparation of the thesis,
- Mr Julyan Symons (Physicist) for his assistance in the neutron beam operation and the writing of the glow curve analysis program,
- Mrs Daphne Commin (Radiographer) for calculating the patients doses,
- The radiographers at NAC for their help with the patient selection and patient set-ups,
- The technicians for making the phantoms ,
- The NAC for providing the facilities and financial support,
- The University of Cape Town Scholarship office for financial assistance and the students at Medical Residence (UCT) for encouragement and support,
- Mr Cameron Challens and Mr Jan Hough, the physicists at Groote Schuur Hospital for their encouragement and support,
- To my family, colleagues and friends who assisted in different ways in the completion of the thesis.

This thesis is dedicated to my father

"Ziyof' izinsizwa, kuyosal' izibongo"

Declaration

I, the undersigned, hereby declare that the work contained in this thesis is my own original work and has not previously in its entirely or in part been submitted at any university for a degree.

Signature ..... Signed by candidate

Date: ..... 10-03-2020 .....

Abstract

Thermoluminescent detectors (TLD-700) have been investigated for absorbed dose measurements in a p(66)/Be neutron therapy beam at the National Accelerator Centre. Chips were selected based on their reproducibility and chip individual neutron calibration factors were derived. The dose non-linearity was determined in peak 5 and peak 6 and dose non-linearity corrections were performed. The sensitivity of TLD-700 chips with depth and off-axis distance was determined. In-vivo dose measurements were performed on seven patients (9 fields). In the entrance in-vivo dose measurements, a maximal deviation of 3.2 % was detected and a systematic difference of 1.7 % was observed. On the exit side, a maximal deviation of –7.3 % was detected and a systematic difference of –5.1 % was observed. The glow curve peak 6/5 ratio was investigated and found to correlate with the qualitative variations of the average LET in the neutron beam.

Table of Contents

Chapter 1: Introduction

1.1 Introduction to the project

The use of radiation in the treatment of cancer patients relies on the precise and accurate delivery of the prescribed radiation dose to the designated planning target volume. A variety of quality assurance procedures are routinely employed to guarantee the proper operation and utilisation of the equipment and to ensure the safe delivery of the radiation dose. In addition, the measurement of the actual dose received by the patient during treatment can be used as an ultimate check of the whole treatment planning and delivery chain. This procedure, known as in-vivo dosimetry, can detect errors that may otherwise be unnoticed. For example, Leunens *et al.* (1990) detected inaccuracies in the planning algorithm and the dosimetry procedures after implementing an extensive in-vivo dosimetry program. In addition, errors in the patient positioning and the set-up of treatment parameters were detected in this study. The implementation of in-vivo dosimetry

is therefore a worthwhile addition to any quality assurance program and can increase the confidence level of radiotherapy procedures.

At the National Accelerator Centre (NAC), near Cape Town, patients are routinely treated at a p(66)/Be fast neutron therapy facility. The accuracy and precision requirements for neutron therapy match those for photon therapy (Mijnheer *et al.*, 1987) and similar quality assurance procedures are recommended. Thus far, in vivo dosimetry is not employed at the neutron therapy facility and it is the aim of this project to develop and implement this procedure at the NAC neutron therapy facility.

Initial measurements were performed to establish the feasibility of using LiF thermoluminescent dosimeters (TLD-700) to determine the absorbed dose in phantom. In vivo dosimetry was then performed on several patients where entrance and exit doses were measured. Results were compared to the calculated absorbed doses according to the treatment plan. Furthermore, glow curve analysis was used to characterise the relative response of glow curve peak 6 to that of peak 5. This glow curve peak ratio is known to depend on the linear energy transfer (LET) (Noll *et al.*, 1997). The variation of peak 6 to peak 5 ratio was investigated in our neutron beam and compared to expected qualitative changes in the beam. The remainder of this chapter will introduce in-vivo dosimetry,

neutron therapy, thermoluminescent dosimetry in general, and thermoluminescent dosimetry for in-vivo measurements in neutron therapy.

1.2 In- vivo dosimetry

Radiotherapy treatment techniques require a series of stages ranging from basic dosimetry over tumour localisation, treatment planning, and dose calculation to the daily irradiation of the patient with multiple fields. Each step involved is subject to a certain degree of uncertainty that can lead to possible discrepancies between the prescribed and the delivered dose. To minimise errors in each step, quality control procedures are required. In-vivo dosimetry is often an integral part of the quality control program since it allows a comparison of the treatment plan dose with the actual absorbed dose received by the patient.

According to ICRU Report 24 (1976), in-vivo dosimetry can be divided into three categories: entrance dose, exit dose and intra-cavitary or organ dose measurements. Entrance dose measurements can be used to check the patient set-up, beam parameters and the machine output performance. Entrance dose measurements allow the comparison of the planned dose with the actual delivered dose. It is usually performed on the patient skin with suitable build up material. Exit dose measurements can be used to perform similar checks and can give information about the treatment planning accuracy. These measurements are

usually performed on the patient skin on the central axis of the beam exit. Intra-cavitary and organ dose measurements can be performed on the accessible structures of the body to check that the received dose is in agreement with the calculated dose. Intra-cavitary in-vivo dosimetry has been performed at many sites of the human body such as mouth, oesophagus, uterus, cervix and the rectum (Cameron, 1968).

Various dosimetric methods are available for in-vivo dosimetry. Most in-vivo dosimetry is performed either with diodes or with TLDs. Semiconductor diodes (Alex *et al.*, 1999) are widely used as in vivo dosimeters. The advantages of using semiconductor diodes are their small physical size, the ease of handling, and the ability to give an online readout. A disadvantage is that cables need to be attached to the diodes.

Thermoluminescent dosimeters are a widely used and versatile tool for the assessment of dose from ionising radiation. In photon beam dosimetry, they have been used widely to measure entrance and exit doses on patients for localised (Loncol *et al.*, 1996) and whole body irradiations (Amor *et al.*, 1998). The small physical size and the fact that no cables or auxiliary apparatus is required during irradiation allow their use in many sites of the body. In-vivo dosimetry with ionisation chambers has been performed by Heukelom *et al.* (1991). The

disadvantages of this method are the large physical size of the ionisation chamber and the need to supply high voltage.

In neutron therapy dosimetry, various methods have been used for in-vivo dosimetry. The use of silicon diodes for in-vivo dosimetry in neutron therapy beams was investigated by Smith *et al.* (1977) and Page *et al.* (1984) in d(50)/Be and d(16)/Be beams respectively. The sensitivity of the diodes depends on the neutron spectrum and the accumulated dose. Corrections for temperature dependence at readout and fading need to be implemented. Only part of the radiation damage can be reversed by annealing the diode, which limits their re-usability. However, after applying the required corrections, both studies concluded that the silicon diodes could be used to measure the neutron dose with a precision of 5 %.

In-vivo dose measurement using ^{27}Mg activity induced in small pellets of aluminium has been performed by Field et al. (1984) for intra-cavitary dose measurements using a d(14)/T neutron beam. The method was tested in a phantom and was later used as a routine check of the dose distribution in clinical trials. The results were in agreement with ionisation chamber measurements. Blake *et al.* (1990) investigated the use of TLD and activation detectors for in-vivo dosimetry in a p(62)/Be fast neutron therapy beam. They found that the former provides a more accurate estimation of the total absorbed dose in a high-

energy neutron beam. In-vivo dosimetry using $CaSO_4$ TLD dosimeters has been performed by Blum *et al.* (1976), on patients treated with a d(16)/Be neutron beam.

1.3 Neutron therapy

1.3.1 Rationale

Neutrons are indirectly ionizing particles, i.e. their energy is deposited in a target material in a two-stage process. In a first step, the neutrons interact with the nuclei of the target material and secondary particles are generated. In a second step, these secondary particles ionize the target material as they transfer their energy to the material. In tissue, the predominant neutron interaction is elastic scattering of hydrogen nuclei. At high neutron energies (above 10 MeV), inelastic and non-elastic scattering reactions gain significance. In fast neutron therapy, the secondary charged particle spectrum in tissue consists of protons, alpha particles and heavy nuclear particles. These secondary charged particles have a high linear energy transfer (LET) value relative to that of electrons (ICRU 36, 1983). The LET or stopping power is defined as

$$\text{LET} = dE/dl$$

where dE is the mean energy lost by a charged particle in collision along an element *dl* of its trajectory (Hall, 1988). The LET of secondary charged particles increases with increasing particle charge and decreasing speed. The dependence

of LET on particle type and energy is shown in figure 1.1. Due to the high LET of the secondary charged particles generated, neutrons are generally referred to as high LET radiation.

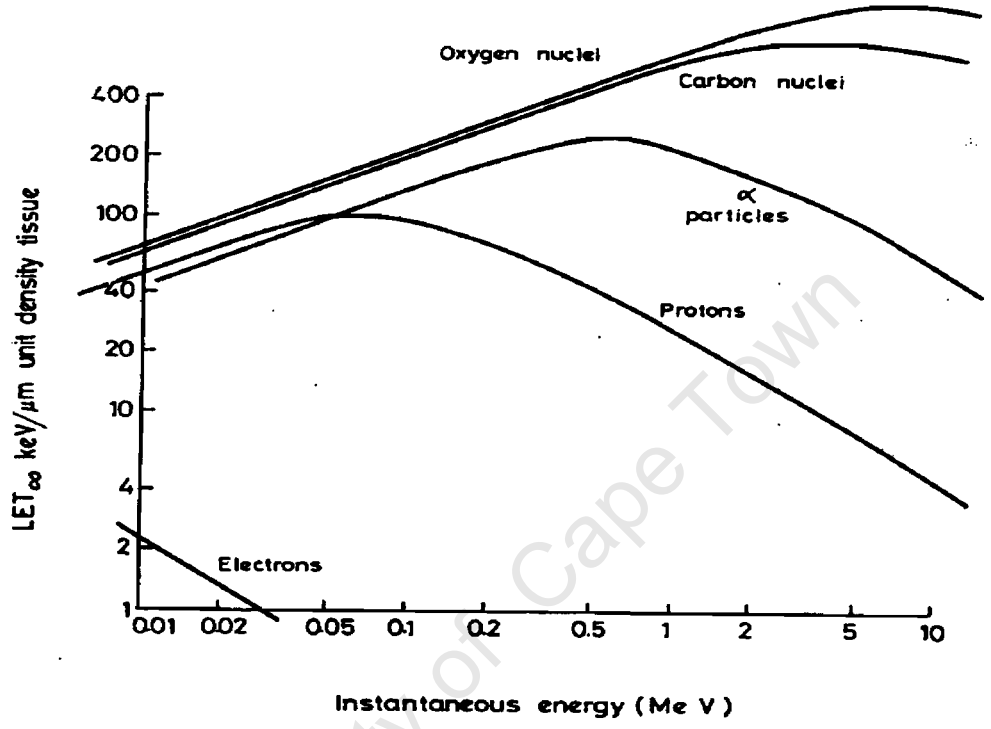

Figure 1. 1: LET of various secondary particles as a function of energy (Bewley, 1989)

The relative biological effectiveness (RBE) of a neutron beam is defined as the ratio of the dose of a reference photon beam to the dose of neutrons required to achieve an equal biological effect. The RBE is a function of the LET. What has been observed is that for a variety of mammalian cells, the RBE first rises to a maximum at about 100 keV per micron and then falls as the LET increases (Bewley, 1989). The peak in the curve of LET versus RBE corresponds to the

optimal level of LET required for cell killing. After this point, a further increase in LET results in a decrease in RBE, as the additional energy deposited no longer contributes to cell killing because of the overkill effect. After this point, additional deposited energy is wasted (Hall, 1988). Figure 1.2 illustrates experimental findings with mammalian cells.

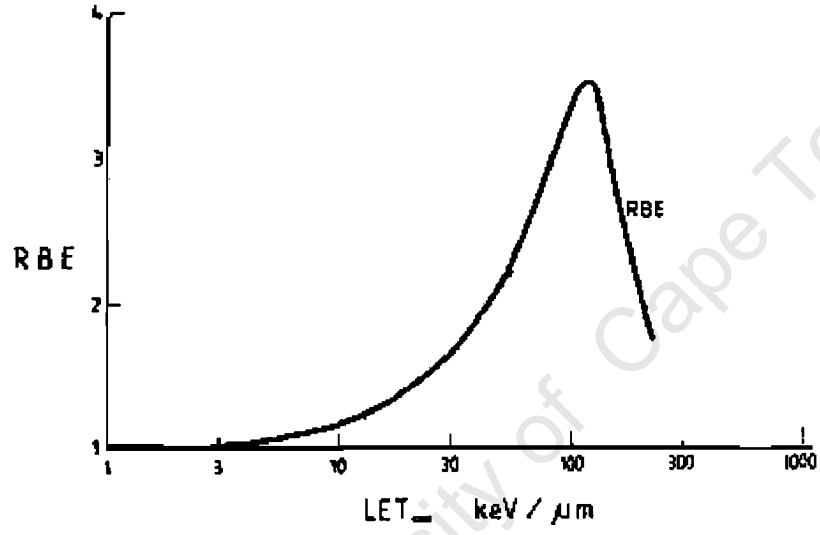

Figure 1. 2: Variation in RBE with LET (Modified from Bewley, 1989)

Earnest Lawrence, the inventor of the first cyclotron introduced neutron therapy in 1938 in the USA, six years after the discovery of neutron. The radiobiological information available at that time was inadequate and provided no definite rationale for using neutrons in preference to x-rays. The observed late effects were greater with neutrons than with x-rays and many patients suffered severe

late reactions (Stone, 1948). Consequently, the use of fast neutrons in radiotherapy was abandoned for nearly 30 years (Raju, 1996).

The rationale for re-introducing neutron therapy at the Medical Research Council in England can be summarized as follows:

- The oxygen enhancement ratio (OER) is defined as the ratio of the dose required to obtain a radiobiological effect when the irradiation is performed under hypoxic versus oxygenated conditions. The value of OER for x-rays is about 3 and this value is reduced to 1.6 for neutrons. This implies that hypoxic cells are less effectively protected when treated with neutrons than with photons. Large tumours often contain a significant fraction of hypoxic cells and should respond favourably to neutron irradiation (Wambersie, 1992).

- The radiation sensitivity changes with phases of the cell cycle. With neutrons, there is less variation in the radiosensitivity between the cell phases. In tumours that are slow growing, the cells spend a longer time in the resting phase of the cell cycle, where they are relatively insensitive to photon radiation. These tumours are relatively resistant to conventional photon radiation but are less resistant to neutron irradiation, which therefore in principle has a better chance of effecting a cure (Raju, 1996).

Investigations by radiobiologists provided clues regarding the types of tumours that are suitable for treatment with fast neutrons. They found a wide range of neutron RBE values for tumours that exceed the range for normal tissue (Wambersie, 1992). Examples of tumours that are effectively treated with neutrons include salivary gland tumours, advanced breast tumours, head and neck tumours and certain tumours of other soft tissues. The types of tumours mentioned above and others are associated with 10 – 15% of radiotherapy patients (Wambersie, 1992). Therefore, it is important to properly select those patients for neutron therapy that are expected to benefit from it.

1.3.2 The neutron therapy facilities

Few fast neutron therapy facilities are currently in operation worldwide. In fast neutron facilities, neutrons are produced by protons or deuterons of energies above 30 MeV (Wambersie *et al.*, 1999). The depth dose distribution of these beams is comparable to those achieved by 6 - 8 MV x-ray beams generated by linear accelerators. Isocentric gantries and multi-leaf collimators are installed at some facilities. The fast neutron therapy facilities that are currently in operation are listed in table 1.1. More than 25000 patients have been treated with neutrons worldwide to date (Jones, 1999).

Country	Place	Reaction	Comments
Belgium	Louvain-la-Neuve	p(65) + Be	Vertical beamline, multileaf collimator
China	Beijing	p(35) + Be	Horizontal beam line, inserts
United States	Seattle	p(50) + Be	Isocentric gantry, multileaf collimator
United States	Batavia IL	p(66) + Be	Horizontal beam line, inserts
United States	Detroit	d(50) + Be	Isocentric, multo-rod collimator
France	Orleans	p(34) + Be	Vertical beamline, Inserts
South Africa	Faure	p(66) + Be	Isocentric gantry, multileaf collimator
South Korea	Seoul	p(50) + Be	Isocentric, variable jaws

Table 1. 1: Currently operational fast neutron therapy facilities (Modified from Wambersie et al., 1999).

The National Accelerator Centre, at Faure in South Africa is the only neutron therapy facility in the southern hemisphere (Jones *et al.*, 1995). Treatment of cancer patients at NAC began in 1989 on the p(66)/Be neutron therapy unit. A total of 1112 patients have been treated since then (Jones, 1999). Some of the tumours that are treated at NAC are head and neck tumours, salivary gland carcinoma, breast tumours, soft tissue sarcomas, uterine sarcomas, paranasal sinuses tumours and mesotheliomas (Stannard, 1998).

The NAC facility is equipped with a separated sector cyclotron that can accelerate protons up to an energy of 200 MeV. This facility was planned specifically to provide research opportunities in natural sciences for users from all over the country and other parts of the world, to supply high-energy particles

for radiation therapy, and to produce radioisotopes for medical use. Figure 1.3 illustrates the layout of NAC's major facilities.

Neutrons are produced by bombardment of a 19.6-mm thick beryllium target with 66 MeV protons. The proton beam dissipates 40 MeV of energy in this target and the remaining energy is lost in a copper backing and in the cooling water. An isocentric gantry is capable of rotating the beam by ±185 degrees. A collimator with a continuously variable rectangular aperture provides field sizes between 5.5 cm x 5.5 cm and 29 cm x 29 cm at a source-to-axis distance of 150 cm.

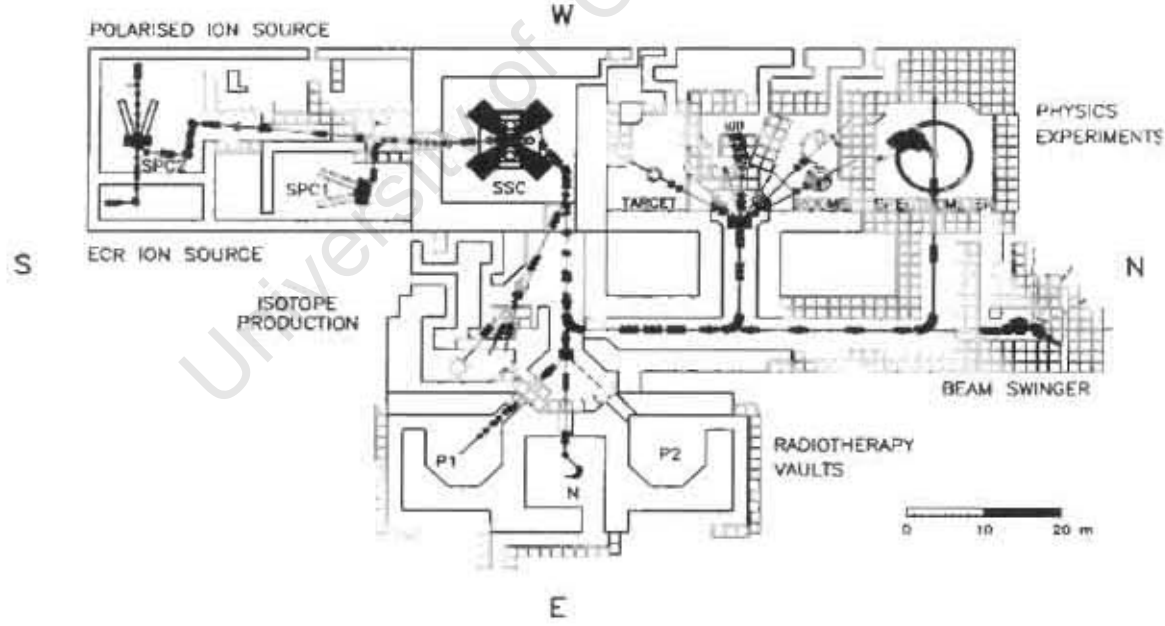

Figure 1. 3: Layout of NAC facility

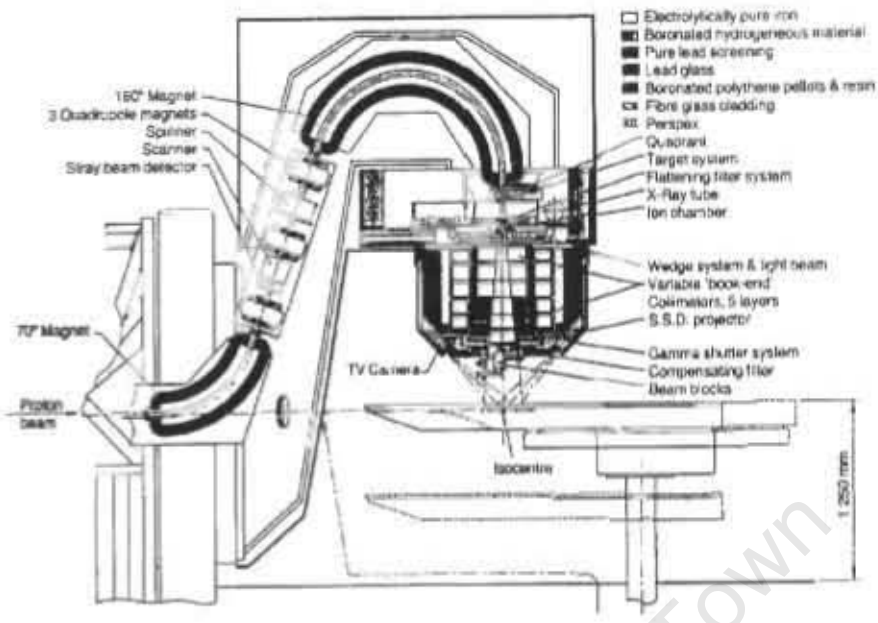

Figure 1. 4: The NAC's neutron therapy isocentric gantry

A multiblade trimmer, which permits the adjustment of the size and the shape of the neutron field to match the size and shape of the tumour, has been installed (Jones *et al.*, 1997). A diagram of the gantry, which shows all the components, is shown in figure 1.4. A detailed description of the NAC facility can be found in Jones *et al.* (1994), Jones *et al.* (1995) and Jones *et al.* (1999).

The penetration of the NAC neutron beam in tissue is similar to that of 8-MV x-rays generated by a linear accelerator. The percentage depth dose curve of the NAC p(66)/Be neutron beam and 8 MV x-rays is shown in figure 1.5. The neutron dose rates are in the range of 0.30 - 0.45 Gy/min (Jones *et al.* 1995).

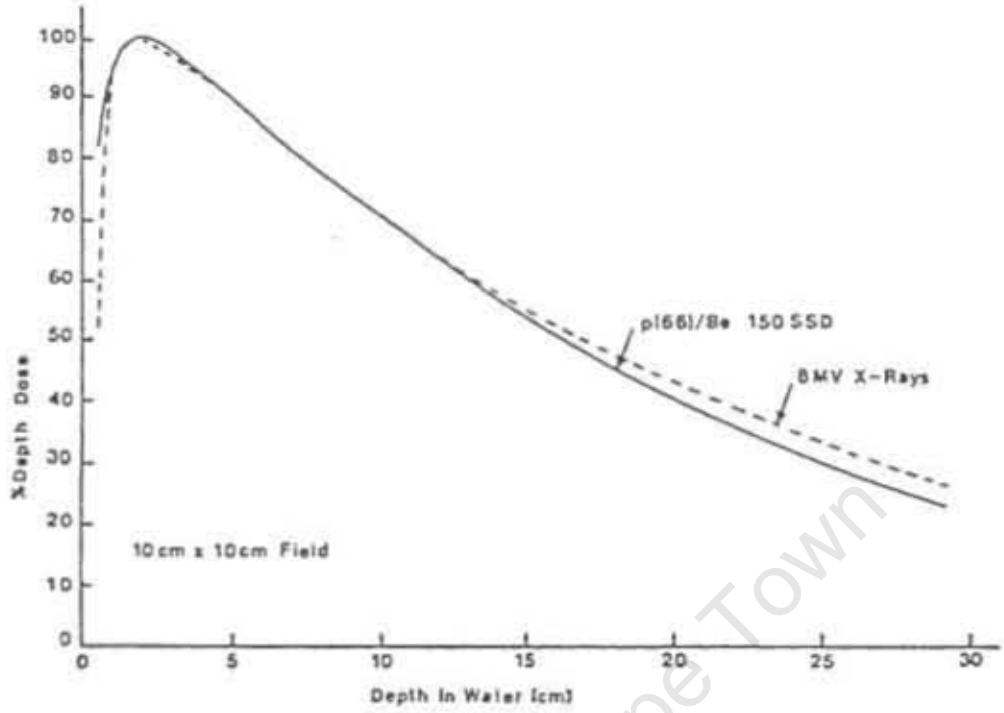

Figure 1. 5: Central axis percentage depth dose of a p(66)Be neutron and 8 MV x-ray beams (Modified from Jones et al., 1989).

1.4 Thermoluminescent dosimeters

1.4.1 Principle of operation

Some crystalline materials, when irradiated by ionising radiation, store part of the energy absorbed in the crystal lattice. When the crystal is subsequently heated, part of the stored energy is released as visible light. The amount of light released is proportional to the amount of ionising radiation the detector has been exposed

to. The light that is released can be collected and measured by a photomultiplier tube. The phenomenon of visible photons released by thermal means is called thermoluminescence. Thermoluminescence has been observed for centuries when certain fluorides and limestone have been heated (Cameron *et al.*, 1968).

The simple model of thermoluminescence is illustrated in figure 1.6. In a pure crystalline substance at room temperature, the conduction band is completely empty and all electrons reside in the valence band. The valence band and the conduction band are separated by a forbidden gap. The presence of impurities in the crystal may create energy traps in the forbidden gap, which may provide metastable states. When the crystal is irradiated, some of the electrons receive sufficient energy to move to the conduction band leaving a hole in the valence band. The electrons and holes are free to move in the crystal until they recombine or become trapped in the metastable states. If the crystal is heated, the electrons can acquire sufficient thermal energy to escape the trap, and move to the conduction band from where they may fall to the valence band. This transition may result in the emission of light. A plot of the light output against temperature is called glow curve (Khan, 1994). Figure 1.7 shows a graph of the temperature and the thermoluminescence (TL) output versus time.

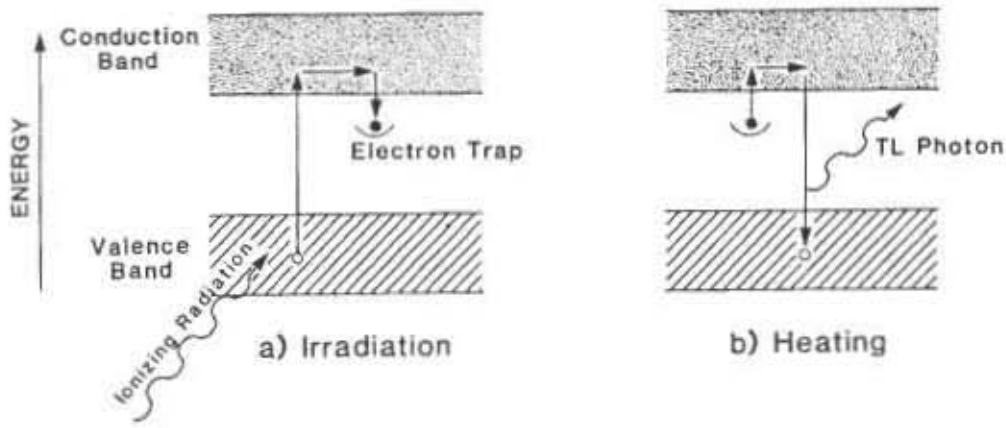

Figure 1.6: Irradiation and heating stages of a thermoluminescence process (Khan, 1994).

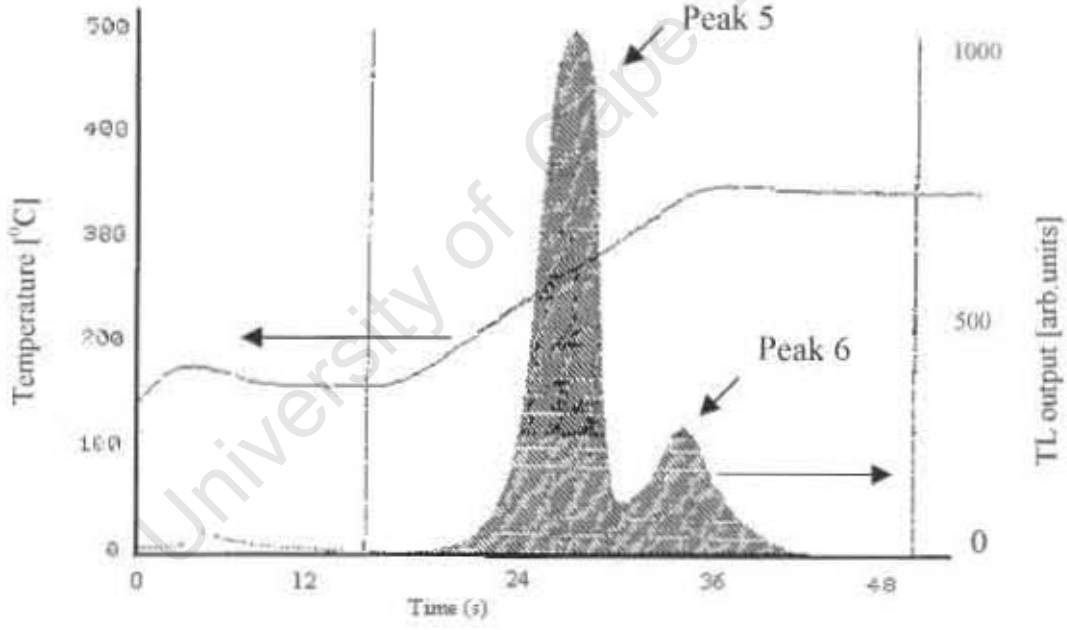

Figure 1. 7: A TLD-700 glowcurve showing the variation in temperature and TL output with time.

A real phosphor normally consists of more than one trapping centre, each trapping centre caused by a particular lattice defect. Each trapping level gives

rise to an associated glow peak. The area and height of each glow peak depends on the number of associated electrons traps present, which in turn depend on the number of lattice defects. The factors that may affect the shape of the glow curve include the following: the heating rate, size, shape and thermal conductivity of the sample, the recording instrument used, the radiation type and annealing procedure (Cameron, 1968, McKinlay, 1981).

1.4.2 Advantages and disadvantages of TLD

The advantages and disadvantages of TLD have been discussed by Kron (1999), and can be summarized as follows:

The advantages are as follows:

- TLD has a linear dose response over a wide dose range.
- The effective atomic number of TLD is approximately equal to that of tissue, which is important for photon dosimetry where the absorbed dose is a function of the effective atomic number of the material.
- As integrating dosimeters, they can measure doses over a long period of time.
- Reusable, after applying appropriate annealing procedures to release the stored energy.

- The fact that no auxiliary equipments are needed during irradiation enables TLD to be used as in-vivo dosimeters and in medical physics, personnel dosimeters, and as area monitors in health physics.
- The glowcurves provide the means of extracting additional information from TLD readings as the ratio of the different peak intensities are related to LET.

The disadvantages are as follows:

- There are no lasting records except for a glowcurve and integrated output.
- They are sensitive to exposure by ultraviolet light and therefore must be kept in a dark environment.
- Expensive readout equipment is required to evaluate the detectors.
- TLDs require calibrations because they are not absolute dosimeters.

1.4.3 Application of TLD

Different types of TLDs can be used for different applications in health and medical physics. For environmental monitoring, TLDs are employed for the measurements of radiation exposure from cosmic radiation exposure in high altitude aircraft (Noll *et al.*, 1999), terrestrial radiation in soil and rocks, and accidental release of man-made radioactivity (McKinley, 1981). The system is also employed in atomic energy centres and isotope laboratories for personnel and area monitoring (McKinley, 1981).

The wide applications in medical physics include diagnostic and therapeutic purposes. In diagnostic radiology, TLDs are employed to investigate the radiation exposure in computer tomographic scans (Smith *et al.,* 1998), mammography, and x-ray examinations. In radiotherapy, they are employed for determining the dose distribution in phantom and as in-vivo dosimeters (Kron, 1999).

1.5 In-vivo TLD in neutron therapy

The most commonly used TLD phosphors in radiotherapy are lithium fluoride (LiF) and calcium fluoride (CaF_2). LiF TLDs are available in many forms, like microrods, granules, pellets, and discs. They are available in three different lithium isotope ratios: TLD-100 which contains natural lithium (7.5% ^{6}Li, 92.5% ^{7}Li), TLD-600 which contains ^{6}Li only and TLD-700 which contains ^{7}Li only. ^{6}Li has a high thermal neutron capture cross-section. TLD-100 and TLD-600 are therefore sensitive to thermal neutrons and are both used in personnel neutron dosimetry at reactor and accelerator facilities. For fast neutron in-vivo dosimetry the TLDs should be insensitive to thermal neutrons as their contribution to the dose is insignificant, hence TLD-700 is suitable for in-vivo neutron dosimetry.

Both TLD-300 and TLD-700 have been investigated for use as in-vivo dosimeters in fast neutron therapy (Loncol *et al.,* 1996, Hocini *et al.*, 1988,

Angelone *et al.*, 1998). TLD-300 is perhaps more widely used than TLD-700 for neutron dosimetry and they are the recommended TLDs for high LET dosimetry (Hoffmann, 1996). This recommendation is based on the fact that the response of the high temperature peak of TLD-300 is constant over a wide LET range. The response of the most other TLD peaks decrease with LET. This fact complicates in-vivo dosimetry if the chips are exposed to a beam that differs in LET from the calibration beam. Hoffman *et al.*, 1983 have measured the response of both high and low temperature peaks in TLD-300 and TLD-700 versus the dose mean lineal energy, $\bar{y}_D$ (ICRU 36, 1983). This parameter is related to the average LET of the secondary particle spectrum of the beam. Measurements of $\bar{y}_D$ in a p(66)/Be neutron beam show that $\bar{y}_D$ varies with field size and water depth in the region between 70 – 75 keV/micron (Binns *et al.*, 1988). An analysis of Hoffman's *et al.* (1983) findings reveal, however, that in this $\bar{y}_D$ region both main dosimetry peaks, i.e. the high temperature peak in TLD-300 and the low temperature peak of TLD-700, exhibit a decrease in sensitivity with LET. It can be argued that in the aforementioned region the response of the low temperature peak in TLD-700 varies less with LET than the high temperature peak of TLD-300. This is corroborated by Loncol *et al.* (1996) who observed that in a p(66)/Be beam, the low temperature peak of TLD-700 was the most independent one in terms of beam quality if compared with the TLD-300 peak.

A disadvantage of TLD-700 is the observed supralinearity with dose of its high temperature peak 6 (Rassow *et al.*, 1988). The peak 6/5 ratio of TLD-700 is hence a function of absorbed dose and this dependency has to be corrected for. This can be achieved by mapping the supralinearity of the high temperature peak in the beam of interest. The high temperature ratio of TLD-700 shows a more pronounced dependence on LET than that of TLD-300 (Hoffmann *et al.*, 1983), which is advantageous for high temperature ratio studies. We chose TLD-700 for our studies but this work could also have been performed with TLD-300.

Blum *et al.* (1976) report the use of calcium sulphate ($CaSO_4$: Tm) TLD powder for the dosimetry of patients treated with a d(14)/Be neutron beam at Medical Research Council cyclotron at Hammersmith Hospital. Entrance and exit doses were measured on 50 patients treated mostly for head and neck diseases. At the entrance and exit side, the TLD measurements yielded a mean dose of 1.01 ±0.088 and 0.86 ± 0.17 respectively if compared to the treatment plan dose. An error analysis of the procedure yielded an expected random error of 8 % in the dose determination, which is in agreement with the observed standard deviation of entrance side measurement. The exit dose determination is complicated by transmission of neutrons through the patient and the unknown changes in the energy spectrum at depth. Numerous other authors have investigated and characterised the behaviour of TLDs in neutron beams (Loncol *et al.*, 1996, Angelone *et al.*, 1998, Rassow *et al.*, 1988). However, to the best of our

knowledge Blum's results constitute the only published TLD neutron in-vivo measurements thus far.

1.6 Aims of the thesis

In this project, we intend to measure entrance and exit doses with TLD-700 for patients undergoing neutron therapy at the NAC. The entrance dose will be measured on the patient's skin surface on the central axis of the beam and the measured dose will be compared to the treatment plan dose. At the exit side of the beam, the exit dose will be measured on the skin surface on the central exit of the beam exit. The measured exit dose will be compared to the dose according to the treatment plan.

The peak 6/5 ratio will also be investigated in our beam. The peak 6/5 ratio is the ratio of the thermoluminescence response of peak 5 to that of peak 6. It has been investigated by others and has been found to vary with LET. We will investigate the peak 6/5 ratio behaviour in the field and out of the field of the neutron beam with the aim of extracting further potential information. Variation in peak 6/5 ratio will be compared with variations in beam quality.

Chapter 2: Experimental Methods

2.1 Introduction

In-vivo dosimetry needs to be performed with sufficient accuracy and precision in order to be useful. Only errors that are larger than the accuracy of the dosimetry system can be detected. In modern radiotherapy departments, that employ comprehensive quality assurance programs, an error in the dose delivery larger than 5% can still be expected in up to 1 % of all treatments (Essers *et al.*, 1999). The accuracy of an in-vivo dosimetry system needs to be less than 5% to detect these errors. Carefully calibrated thermoluminescent detector systems can have accuracies of 2 – 5 % and are hence suitably accurate for in-vivo dosimetry (Essers *et al.*, 1999, Kron, 1999).

In an effort to achieve high accuracy and precision, TLD chips were sorted according to their reproducible responses. Chip-specific calibration factors were

determined and used throughout this project. Furthermore, factors that influence the chip sensitivity were carefully investigated and, where necessary, correction factors were determined and applied. In-phantom depth dose and cross-plane measurements were performed and compared with ionisation chamber measurements.

All of the above procedures were aimed at improving the accuracy and precision of the TLD system and to demonstrate its feasibility for in-vivo neutron dosimetry. In this chapter the experimental procedures employed are detailed and the results of in-phantom measurements are presented.

2.2 TLD readout

The reader used for all measurements was a Solaro dual channel TLD processor that contains two readout channels and a drawer mechanism for loading chips. The Solaro is a computer- controlled system consisting of a reader, visual display unit and a keyboard. Round TLD-700 chips of LiF: Mg,Ti (Z_{eff} = 8.2, ρ = 2.6 g/cm^3) (McKinley, 1981) with a diameter of 4.5 mm and thickness of 0.9 mm were used. Before irradiation, the chips were annealed in a computer-controlled oven. The chips were heated to 400 ^{0}C and held at this temperature for one hour. This was followed by twenty hours of baking at 80 ^{0}C before the chips were cooled down to room temperature.

The TLD chips were read 24 hours after irradiation in a nitrogen atmosphere at a heating rate of 10 ^{0}C/s. The heating cycle used was as follows: 15 seconds preheating at 160 ^{0}C, followed by 35 seconds read time, i.e. 20 seconds at 160–350 ^{0}C and constant temperature at 350 ^{0}C for 15 seconds. This is followed by 10 seconds annealing at 350 ^{0}C. The glow-curve data were stored in a computer for subsequent analysis. The thermoluminescence signal versus temperature/time or glow-curves were used to integrate the peaks, peak 5 (200 - 300 ^{0}C) and peak 6 (300 - 350 ^{0}C). Peak 5 is the dominant glow curve peak and therefore was taken as the main dosimetry peak to determine the absorbed dose.

2.3 TLD chip selection and calibration

This section explains the procedures used to select "good" chip with reproducible response from the available ones. Since chip-specific calibration factors are later assigned to all selected chips, the chip's signal reproducibility was chosen as a measure of the chip goodness. This procedure is based on peak 5 only since it is the main dosimetry peak in TLD-700. 200 chips were irradiated with a dose of one gray in the neutron beam. The mean reading over all chips was calculated and the deviation from this mean was calculated for each individual chip. This procedure was repeated three times. The standard deviation of the three deviations from the mean was then computed and this figure was subsequently

used as the measure of the reproducibility of the chip. Although a single chip might show a large deviation from the mean value, it might be a "good" chip because of the reproducibility of its signal. All chips for which the standard deviation (1σ) of the deviations from the mean was better than 3.5% were selected for later use. Exactly 110 chips satisfied this criterion.

For each of the selected chips an individual calibration factor F was calculated as follows;

$$F = \frac{D}{(r_1 + r_2 + r_3)/3}\left[\frac{Gy}{TL\ .signal}\right]$$

where D is the absorbed dose in Gy, i.e. 1 Gy, r_1, r_2 and r_3 are the chip signals due to the first, second and third irradiation.

The TLD chips used in the project were in constant use and the TLD radiation history can change the TLD response. Therefore, all chips were re-calibrated after 12 months. We found that the overall sensitivity of the chips had dropped by 1 to 2 % over this period in which the chips received an approximate accumulative dose of 30 Gy. The observed decrease of sensitivity with continuous use of the chips is in qualitative agreement with studies done by others (Cameron, 1968). The re-calibration of the chips is therefore recommended every twelve months.

2.4 Dose linearity

The chip-specific calibration factors were determined at an absorbed dose level of 1 Gy in the p(66)/Be neutron beam. It can not be assumed that these calibration factors are valid at other dose levels. The dependence of the TLD-700 peak sensitivities on absorbed dose was reported previously (Meissner *et al.*, 1988, Pradhan *et al.*, 1985, Rassow *et al.*, 1988, Waligorski *et al.*, 1980).

To characterise the dose response of TLD-700 in our neutron beam, TLD chips were irradiated with absorbed doses ranging from 0.01 to 3 Gy. For each run 10 chips were placed in a nylon 6 phantom and were irradiated at a water equivalent depth of 2 cm (nylon depth of 1.6 cm). The phantom was made up of nylon slabs that were 10 cm x 10 cm in size (ρ = 1.2 g/cm^3) and 0.8 cm thick (1 cm water equivalent depth). The slabs, which held the TLD chips, had 1-mm deep holes for the TLD chips. After read out the peak 5 reading was converted into response using the individual calibration factors determined earlier. The response of the main dosimetry peak, peak 5, as a function of absorbed dose, is shown in figure 2.1.

The observed saturation effect of peak 5 can not be corroborated by other published findings. Several dose linearity studies in the d(14)/Be neutron beam at Essen confirm the linear response of peak 5 up to the dose of 100 Gy (Meissner

et al.,1988, Pradhan *et al.*, 1985, Rassow *et al*, 1988). Irradiation in a cobalt-60 beam showed a slight supralinear response of peak 5 at an absorbed dose of 100 Gy (Pradhan *et al.*, 1985,Waligorski *et al.*, 1980). Only at an absorbed cobalt-60 dose of 1000 Gy was saturation observed (Waligorski *et al.*, 1980). These findings are in contrast to our observation in the p(66)/Be neutron beam.

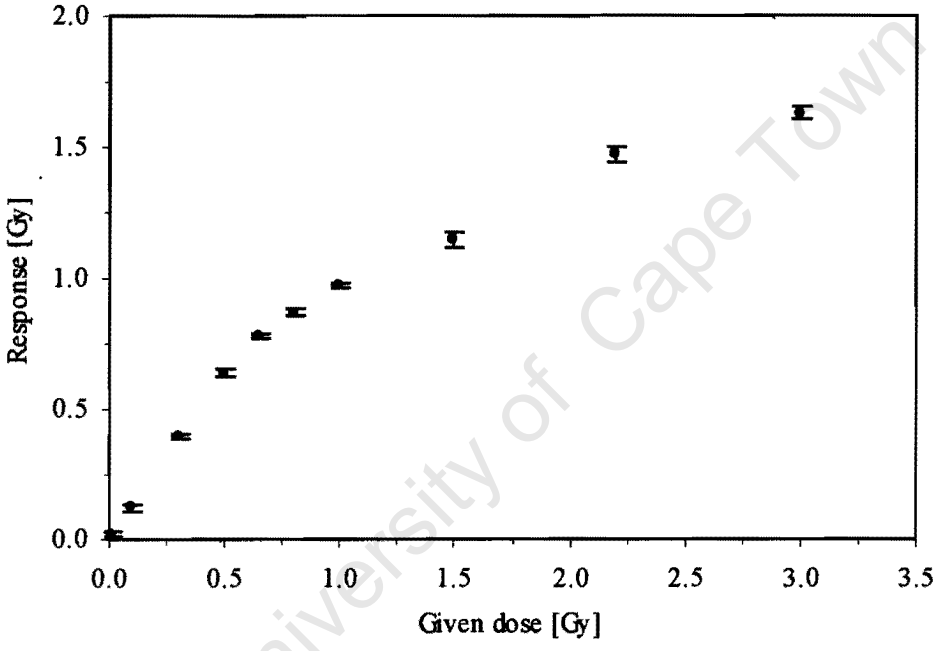

Figure 2. 1: Response as a function of neutron dose of the main dosimetric peak 5. Each data point represents the mean of 10 TLD chips. The error bars refer to the error of the mean (1δ).

It should be remembered that the saturation of the recorded thermoluminescence signal could be due to a reduced thermoluminescent chip output or a saturation of

the light collection apparatus. This was investigated by comparing TLD readings of our reader with those obtained from a reader belonging to a neighbouring hospital. TLD chips were irradiated with cobalt-60 doses ranging from 0.1 Gy to 15 Gy. Chips were read in our Solaro TLD reader. The cobalt-60 irradiations were repeated and the chips were read using the Toledo TLD reader at the Groote Schuur Hospital (GSH) in Cape Town. Figure 2.2 shows the results of both readings. The Solaro TLD reader results exhibit saturation whereas the GSH Toledo results are linear up to 15 Gy. However, since the same thermoluminescent chips and Solaro reader were used for all subsequent measurements, a correction of the observed saturation effect is possible.

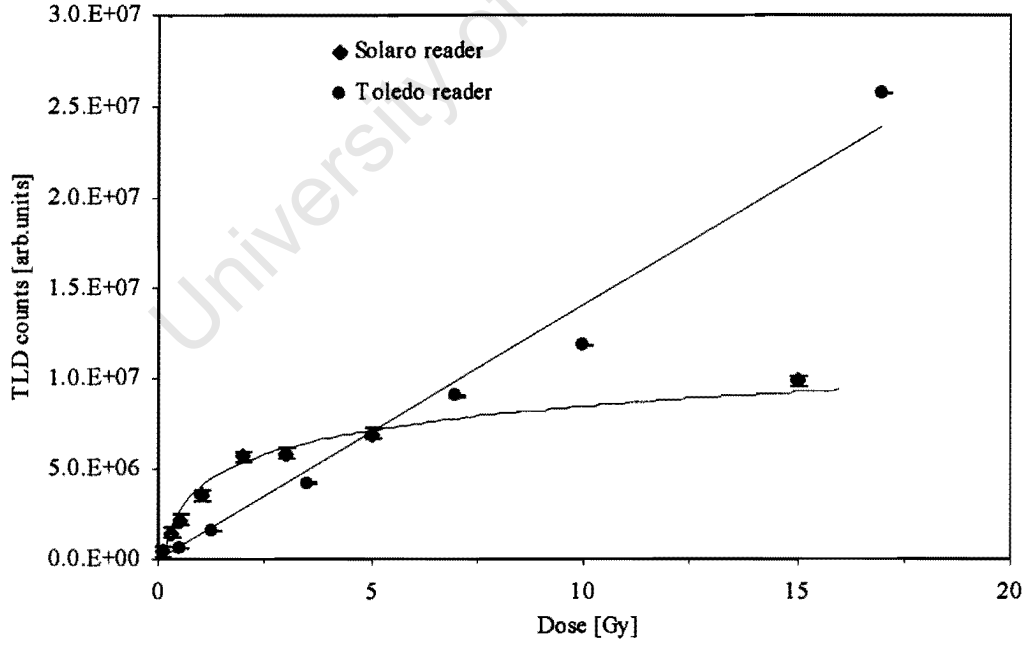

Figure 2. 2: Dose response in cobalt beam for a Solaro and a Toledo reader.

To relate the thermoluminescent response to the absorbed neutron dose for all subsequent measurements a curve fitting routine was used to determine the absorbed neutron dose as a function of the thermoluminescent response. Figure 2.3 (equivalent to figure 2.1 but with reversed axis) shows the absorbed dose as a function of response and illustrates the applied curve fitting routine. The following 7th order polynomial equation was derived:

Absorbed neutron dose $[Gy] = a + br + cr^2 + dr^3 + er^4 + fr^5 + gr^6 + hr^7$

where a = -0.01178, b = 1.357024, c = -5.72469, d = 24.18364, e = -54.3928, f = 64.16435, g = -36.4562, h = 7.878924 and r is a thermoluminescence response in gray.

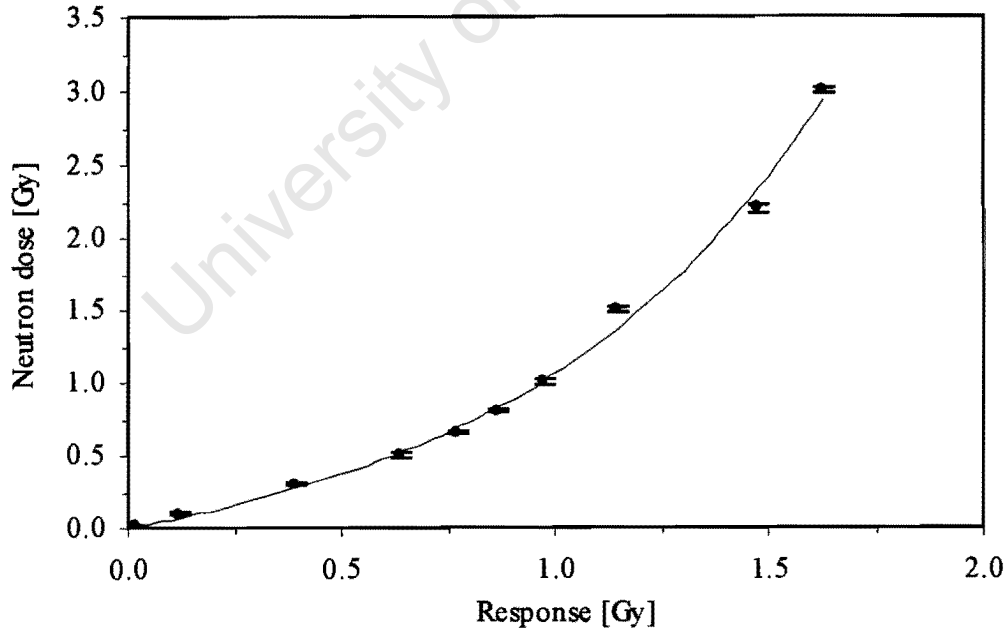

Figure 2.3: Peak 5 dose as a function of response

2.5 Depth dose curves

A neutron beam that is generated by bombarding a semi-thick beryllium target with 66 MeV protons has a wide energy spectrum that ranges from thermal to 66 MeV neutrons (Jones *et al.*, 1995, Awschalom *et al.*, 1983). When this neutron spectrum penetrates into tissue, the lower energy neutrons are preferentially absorbed, which leads to beam hardening at depth (Slabbert *et al.*, 1989, Hornsey *et al.*, 1988). At the NAC p(66)/Be facility a 2.5 cm polystyrene filter is used to harden the beam and therefore to reduce the beam hardening effect in the patient (Jones *et al.*, 1994). However, a remaining beam hardening effect has been observed in the filtered beam. Using microdosimetric measurements, a 6 % reduction in the beam's potency has been detected with depth between 2.5 cm and 20 cm (Slabbert *et al.*, 1989) and between 5 cm and 25 cm (Binns *et al.*, 1992). Changes in the neutron energy spectrum with depth may be of concern for thermoluminescent dosimetry since the sensitivity of TLD-700 is a function of the neutron energy spectrum (Hocini *et al.*, 1988). The aim of the following experiment was to test the magnitude of this effect on the TLD sensitivity and to test whether TLD chips can be used to verify the absorbed dose at different depths in the phantom.

In the experiment the detectors were divided into groups of 8 and stacked in a nylon phantom at different depths ranging from 0 to 20 cm. A diagram of the experimental set up is shown in figure 2.4. For a 5.5 cm x 5.5 cm field, a dose of 1 Gy at 2-cm water equivalent depth was given to the stack. The procedure was repeated at different fields sizes, i.e., 8 cm x 8 cm and 10 cm x 10 cm and 15 cm x 15 cm. For the two smaller field sizes, the phantom size was 10 cm x 10 cm. For the larger field sizes a 20 cm x 20 cm phantom was used. The data obtained were corrected for dose nonlinearly in peak 5 using the equation obtained earlier.

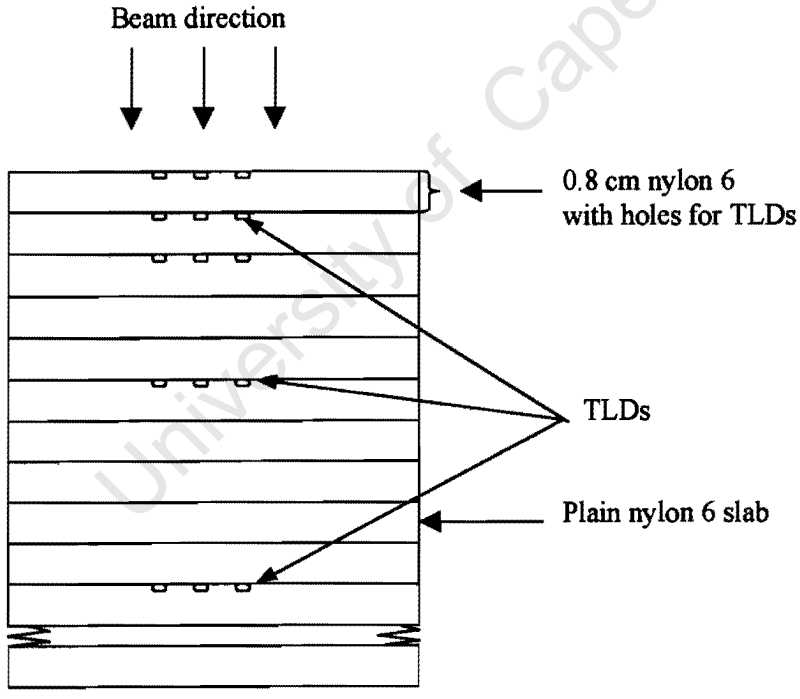

Figure 2. 4: Diagram of the phantom set up. All slabs are 0.8 cm thick. Plain slabs are used to adjust the space between the TLD bearing slabs.

A plot of the absorbed dose measured versus depth for different field sizes is shown in figure 2.5 to figure 2.8. The depth dose distributions obtained with TLD chips were compared with relative ionisation chamber measurements. Numerical results are listed in table 2.1. The TLD data in figure 2.5 to figure 2.8 represent the mean TLD reading over 8 TLDs. The error bars represent the error of the mean (1 δ).

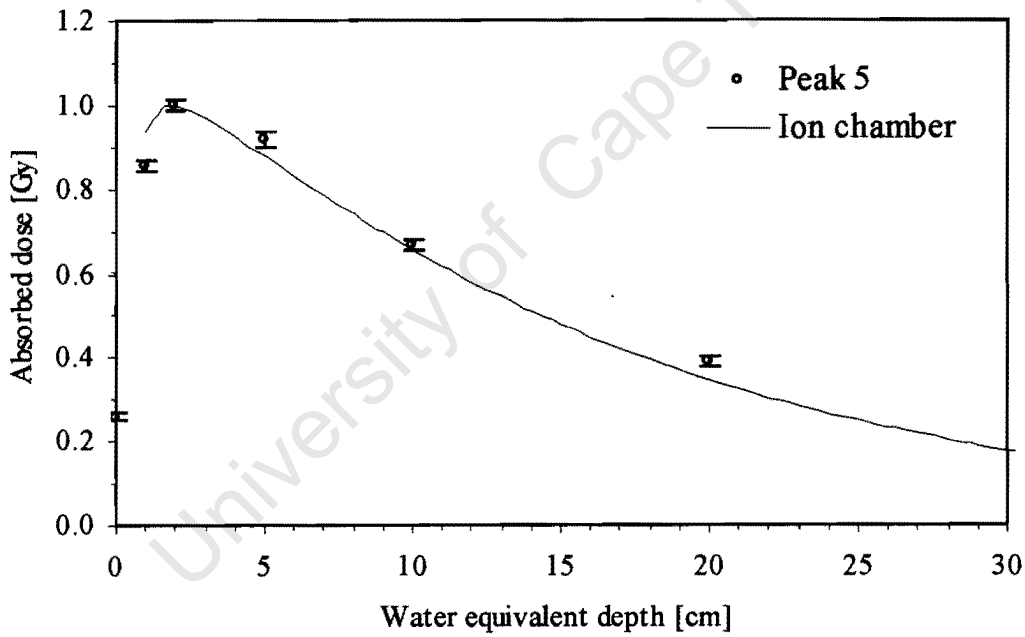

Figure 2. 5: Depth dose curve for a 5.5 x 5.5 cm field

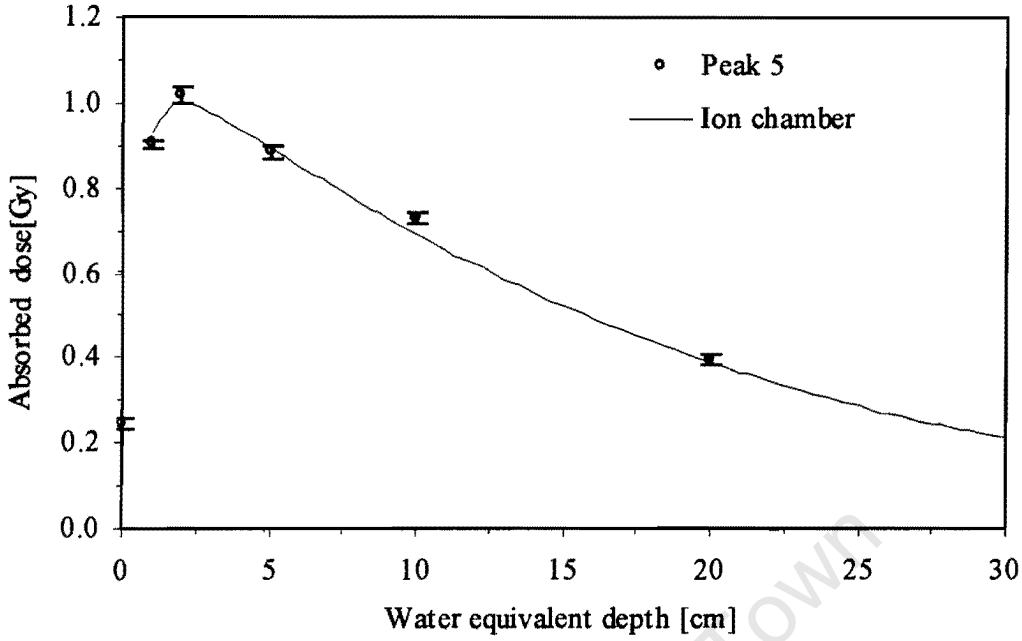

Figure 2. 6: Depth dose curve for a 8 cm x 8 cm field.

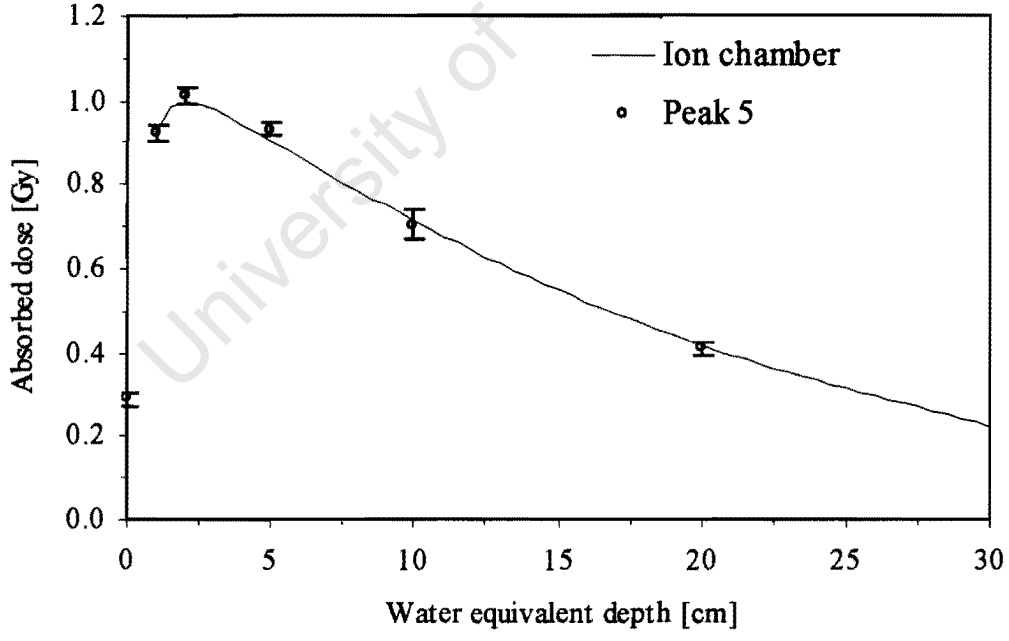

Figure 2. 7: Depth dose curve for a 10 cm x 10 cm field.

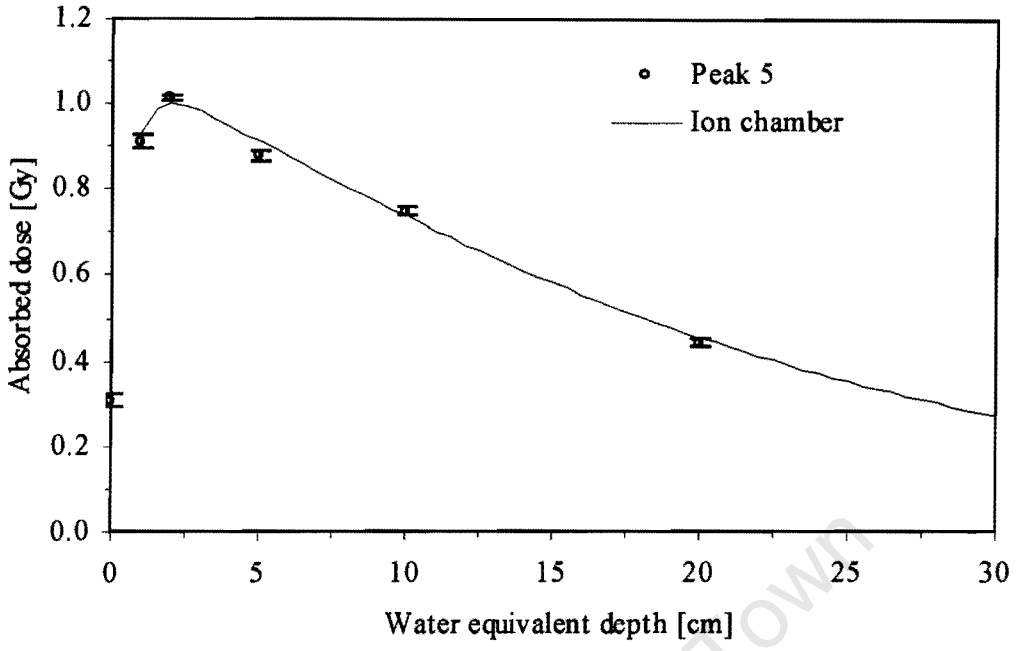

Figure 2. 8: Depth dose curve for a 15 cm x 15 cm field.

Depth [cm]	5.5 x 5.5	8 x 8	10 x 10	15 x 15
1	0.913 ± 0.021	0.971 ± .0017	0.993 ± 0.020	1.035 ± 0.019
2	1.000 ± 0.017	1.018 ± 0.018	1.009 ± 0.019	1.077 ± 0.018
5	1.047 ± 0.023	0.989 ± 0.021	1.031 ± 0.022	1.026 ± 0.017
10	1.015 ± 0.015	1.056 ± 0.017	0.987 ± 0.043	1.029 ± 0.013
20	1.127 ± 0.017	1.043 ± 0.019	0.979 ± 0.034	0.998 ± 0.018

Table 2. 1: The TLD sensitivity in the neutron beam (i.e. TLD dose / ionisation chamber dose) for different field sizes and depths.

The TLD response in two parallel opposed fields has been measured. The experimental set-up is similar to the 10 cm x 10 cm depth dose measurements but

the beam angles were 90 ^{0} and 270 ^{0}. Using two 10 x 10 cm^2 fields at 150 cm SAD, a dose of one gray was given at each angle. The TLD results were compared to ionisation chamber data that was calculated by adding two opposing field depth dose ionisation measurements. Figure 2.9 shows the results.

Qualitatively, an increased thermoluminescence sensitivity at depth may be expected. This is due to two effects. Firstly, $\bar{y}_D$ slightly decreases at depth (Binns, 1993) and the TLD-700 peak 5 sensitivity increases with decreasing $\bar{y}_D$ (Hoffmann *et al.*, 1983). Secondly, the gamma component increases with depth (Jones *et al.*,1995), which again results in an increased thermoluminescence sensitivity to the total dose. With the exception of the smallest field, our results however, show that these effects are negligible in magnitude. Quantitative analysis can corroborate this observation.

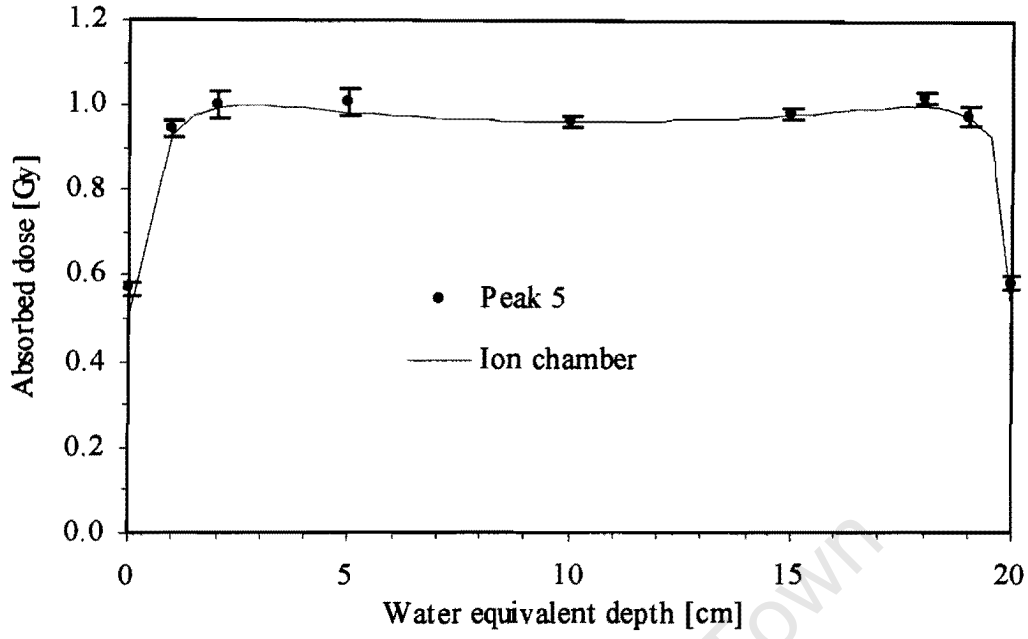

Figure 2. 9: Depth dose curve for two 10 cm x 10 cm parallel opposed fields

Microdosimetric measurements show that $\bar{y}_D$ decreases only slightly with depth from 83.5 – 79.4 keV/μm between 2.5 and 20 cm (Binns, 1993). The gamma component is almost constant with depth in a p(66)/Be neutron beam. It increases from 4 to 6 % from 2 cm to 20 cm depth (Jones *et al.*, 1995). Since the thermoluminescent sensitivity is roughly twice for cobalt-60 than for p(66)/Be neutron beam (Hocini *et al.*, 1988), an increase of thermoluminescent sensitivity of 2 % can be expected. Both above effects are small in magnitude, which is in agreement with our findings. We conclude that the TLD-700 peak 5 can be used to determine the absorbed dose at depth in a p(66)/Be neutron beam.

2.6 Beam profiles

Two processes can affect the overall quality of the neutron therapy beam at the field edges. Firstly, the primary beam softens as a result of beam scattering and secondly, the photon component increases sharply (Binns *et al.*, 1993, Jones *et al.*, 1992). Both effects can influence the thermoluminescence sensitivity in the penumbra region. This experiment was performed to investigate whether TLD-700 chips can be used to measure absorbed doses in the penumbra region of the field.

In the following experiment, measurements were performed in the central axis of the beam and in the penumbra region at a depth of 2 cm. Chips were irradiated in a 5.5 cm x 5.5 cm field and at distance of 1 - 5 cm off-centre. The dose measured in peak 5 is plotted against off-axis distance. The beam profile is shown in figure 2.10 and numerical results are listed in table 2.2.

Binns, (1993) and Jones *et al.*, (1992) performed measurements in the penumbra region at the NAC neutron beam facility. Marked changes were observed in the penumbra region where the photon component was found to increase substantially. The sharp increase in the gamma component should lead to an increased TLD sensitivity in the penumbra region. Our results however, showed a general decrease of TLD sensitivity in this region (Table 2.2). This may be due

to a softening of the neutron component in the penumbra region. A softening of the neutron component leads to an increase $\bar{y}_D$ value (Pihet *et al.*, 1988), and the TLD-700 peak 5 sensitivity decreases with increasing $\bar{y}_D$ value (Hoffman *et al.*, 1983). A quantitative investigation of this effect can be performed with microdosimetric measurements in the penumbra region.

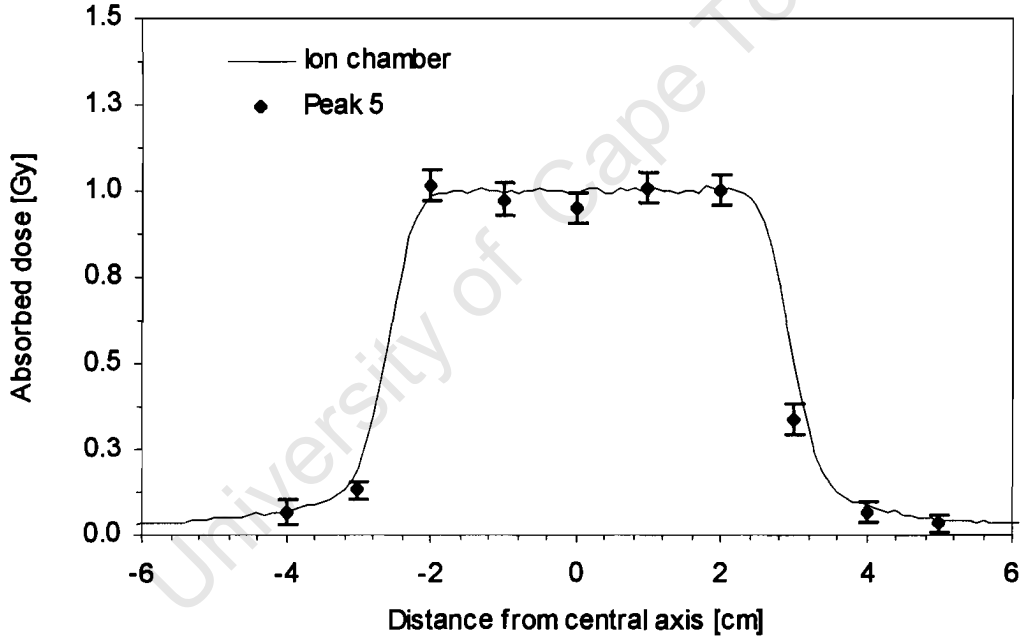

Figure 2. 10: Beam profile for a 5.5 cm x 5.5 cm field.

Lateral distance [cm]	TLD / Ionisation chamber
5	0.741 ± 0.026
4	0.790 ± 0.031
3	0.754 ± 0.042
2	1.002 ± 0.043
1	1.005 ± 0.044
0	0.950 ± 0.040
-1	0.985 ± 0.042
-2	1.031 ± 0.045
-3	0.679 ± 0.026
-4	0.946 ± 0.037

Table 2. 2: The ratio of TLD dose (Gy) and ionisation chamber dose (Gy) with the corresponding distance from central axis. Measurements were taken in a 5.5 cm^2 field at a water equivalent depth of 2 cm.

Chapter 3: In-vivo dosimetry

3.1 Introduction

In-vivo dosimetry can be subdivided into entrance, exit and organ dose measurements (ICRU 24, 1976). Each category has a distinctly different purpose. The measurement of entrance dose is perhaps the most common case of in-vivo dosimetry. Here the dose that the patient receives at a point on the field entrance side of the body is determined and compared to that calculated in the treatment plan. Errors in patient positioning, patient set-up and machine parameters can in principle be detected.

In-vivo dosimetry of exit doses is complicated by the fact that the calculations of the exit dose need to account for the body's inhomogeneities. Unless this is properly done discrepancies between the measured and calculated exit dose can be expected. Hence, exit dose in-vivo dosimetry can be used to gain information

about the validity of the treatment plan calculations rather than to detect set up errors.

Organ dose measurements are employed to measure the dose to organs that are accessible. This can be done in the radiation field or outside the field boundaries. In the latter case, complications arise in neutron therapy due to the qualitative changes of the neutron beam in the penumbra region.

In the previous chapter we have established the feasibility of using TLD for in-vivo dosimetry in the radiation field. Actual in-vivo measurements were performed in 9 fields (7 patients) where entrance and exit doses were measured in the direct radiation fields.

The planning of the treatments was performed on the Theraplan computerised planning system at Groote Schuur Hospital. All treatment planning and patient set-ups were performed by the radiographers. Most of the patients that participated in the study were treated for head and neck diseases. Field sizes varied from 6.7 to 10.7 equivalent square centimetres with and without wedge filters. All fields were adjusted in shape using a multi-blade trimmer (Jones *et al.*, 1997). The treatment plan doses were calculated from the treatment plans and were in the range of 0.46 Gy to 1.3 Gy. Paraffin wax lined with lead was used as a bolus material in most treatments. Wax is less dense than water (0.93 g/cm^3),

has higher hydrogen content (14.6 %), and is therefore similar to water in terms of neutron attenuation (Hess *et al.*, 1991). The bolus is placed directly on the skin surface to smooth out irregular contours of the patient to present a flat surface normal to the beam. The lead lining is used to recover the skin dose that is lost due to the presence of tissue compensator (Hess *et al.*, 1991, Jones *et al.*, 1988). In situations where the wax was used, the detectors were taped to the surface of the wax on the central axis of the beam. Table 3.1 details the patient set up during treatment.

Field no.	Field size (cm x cm), Wedge	Site	Wax	Lead lining	# of session/ total
1 A	8 x 17	Head & neck	Yes	Yes	7/12
1 B	8 X 17	Head & neck	Yes	Yes	7/12
2	7 x 12.5, W2	Lumbar spine	No	No	4/12
3	5.5 x 8.5, W2	Head & neck	Yes	Yes	5/12
4 A	9 X 5.5, W2	Head & neck	Yes	Yes	9/12
4 B	9 x 6.5, W2	Head & neck	Yes	Yes	9/12
5	7.5 x 9, W2	Head & neck	Yes	Yes, except over scar	11/12
6	7.5 x 9, W2	Head & neck	Yes	yes	9/12
7	10 x 11, W3	Head & neck	Yes	Yes, except next to nose	7/12

Table 3. 1: Details of patient set up during treatment. The W2 and W3 refer to the wedge number. The wedges W2 and W3 are 35 and 45 degree wedges respectively. The last column gives the number of the session when the in-vivo dosimetry was performed out of the total number of sessions.

3.2 Entrance dose measurements

Discrepancies between the actual patient or machine set-ups and those used in the treatment plan will lead to a difference in measured and planned absorbed dose. For example, Leunens *et al.* (1990) detected errors in patient positions, patient set up, external patient contours and errors due to the repeated treatment interruptions by means of entrance in-vivo dosimetry.

In-vivo entrance measurements were performed on the patient's skin surface or on the patient's mask surface. For entrance dose measurements we used a 2 mm thick A150 plastics (ρ = 1.12 g/cm^3) as a build up material to avoid the "peak 6/5 ratio" in the glowcurve at the surface as it makes peak 5 read-out more difficult. Chapter 4 explains the high temperature ratio method in detail.

The dose given to the patient according to the treatment plan is defined at a depth of 2 cm. Hence, a mechanism was needed to relate the dose at 2 cm to the dose measured at the patient surface under 2 mm A150 plastic build up. It is the aim of the following experiment to measure the dose at 2 mm depth relative to that at 2 cm depth for different field sizes. At the surface of a nylon-6 phantom and at a depth of 2 cm, measurements were performed for field sizes ranging from 5.5 cm x 5.5 cm to 29 cm x 29 cm. For these phantom measurements, the 'surface' TLDs

were covered with 2 mm A150 tissue equivalent plastic. Figure 3.1 shows a diagram of the experimental set up.

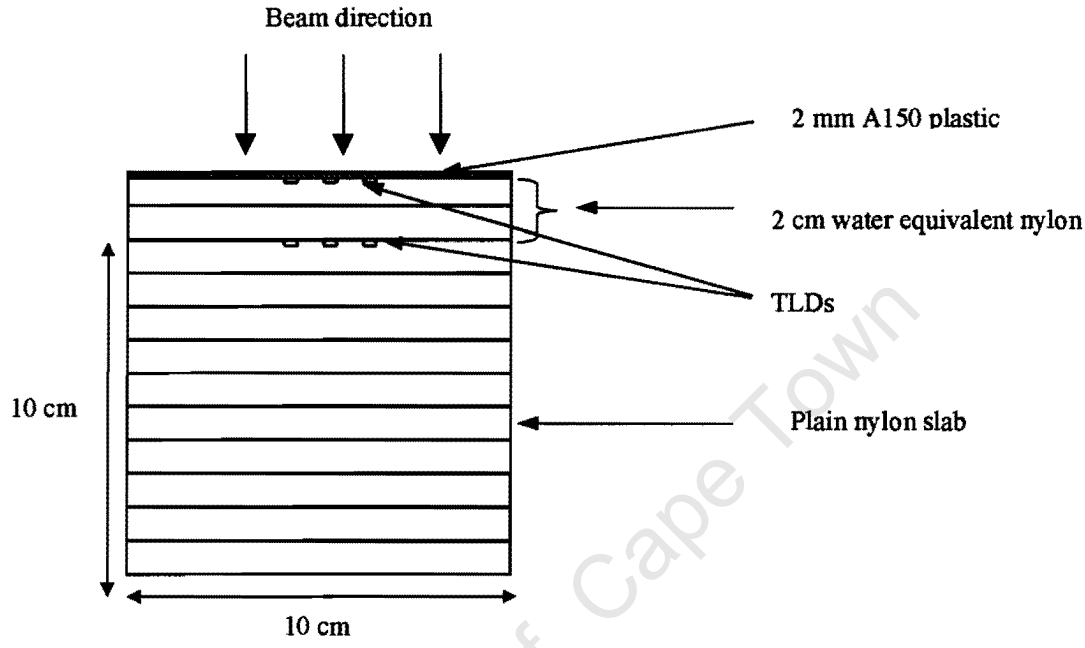

Figure 3. 1: Diagram of the experimental set up.

A plot of square field size versus relative dose measured at 2 mm depth is shown in figure 3.2. An equation that allows calculation of the relative entrance dose as a function of equivalent square field was calculated from the data and was later used in the entrance dose calculation. The equation is as follows;

Relative dose $(EQS) = -0.0102EQS^2 + 0.5699EQS + 53.55$, where EQS represent the equivalent square field.

Awschalom *et al.* (1981) derived an expression for calculating the central axis depth dose in the build up region as a function of equivalent square field in the p(66)/Be beam at Fermilab. We use this expression to compute the relative entrance dose at a depth of 2 mm as a function of equivalent square field for comparison to our results. Figure 3.2 also shows the results obtained by computing Awschalom's expression. Awschalom's results are normalised to ours for the 10 cm x 10 cm field. Both sets of results are in qualitative agreement. The effect of increased relative depth dose at 2 mm depth with increased field size is more pronounced in the Fermilab beam. The Fermilab neutron therapy beam is generated in a thicker beryllium target, i.e. 2.21 cm than the NAC beam and no polyethylene hardening filter is used in the Fermilab beam (Rosenberg *et al.*, 1981).

In-vivo measurements were performed on seven patients (9 fields). For each in-vivo measurement six TLD chips were used. The mean value and standard deviation of the mean are quoted. Entrance dose measurements were performed at the skin surface or on top of the paraffin wax at the radiation field centre. The 2 mm A150 build up slab was cut into size and shape so as to cover six TLD chips. We used the results from the previous experiment to compute the relative entrance dose for each radiation field, which was then used to calculate the dose at 2 cm (100% dose). The determined dose at 2 cm was compared with the

specified treatment plan dose at 2 cm depth. Table 3.2 shows the results for each field.

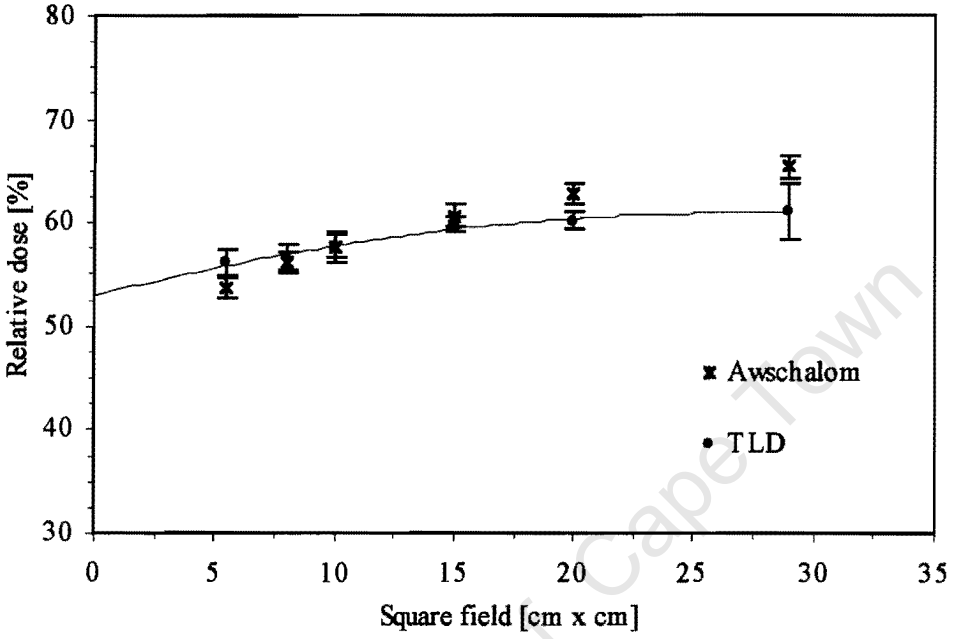

Figure 3.2: Entrance dose as a function of field size. The data represent the mean TLD reading over 5 TLD chips. Awschalom's results are also plotted.

Within the stated experimental uncertainties, all but two in-vivo entrance doses are in agreement with the expected absorbed doses according to the treatment plan. Large errors (< 5%) were not detected and with one exception all discrepancies were smaller than 3%. The two measurements performed on patient 4 show the two largest discrepancies. No reason is apparent for this.

Averaged over all 9 fields, the TLD measurements are 1.7 % higher than the expected treatment plan doses.

Patient information			**Entrance dose**			
Patient	Field no.	EQS	Measurement	100%	T. plan	TLD / T.Plan
		[cm]2	[Gy]	[Gy]	[Gy]	
Patient 1	1	10.9	0.727 ± 0.003	1.242 ± 0.005	1.226 ± 0.025	1.013 ± 0.021
	2	10.9	0.730 ± 0.009	1.247 ± 0.016	1.226 ± 0.025	1.017 ± 0.024
Patient 2	2	8.8	0.560 ± 0.007	0.978 ± 0.012	0.955 ± 0.019	1.024 ± 0.024
Patient 3	2	6.7	0.681 ± 0.007	1.197 ± 0.012	1.189 ± 0.024	1.007 ± 0.022
Patient 4	2	7.5	0.607 ± 0.004	1.060 ± 0.007	1.035 ± 0.021	1.024 ± 0.022
	1	6.8	0.716 ± 0.004	1.257 ± 0.008	1.218 ± 0.024	1.032 ± 0.022
Patient 5	3	8.2	0.663 ± 0.007	1.152 ± 0.013	1.126 ± 0.023	1.023 ± 0.023
Patient 6	3	8.2	0.648 ± 0.019	1.126 ± 0.033	1.126 ± 0.023	1.000 ± 0.036
Patient 7	4	10.5	0.275 ± 0.012	0.471 ± 0.021	0.466 ± 0.009	1.012 ± 0.050

Table 3. 2: Entrance dose measurements. EQS refers to the equivalent square field obtained from treatment charts. The surface dose was measured at the patient skin surface under 2-mm A150 plastic. The 100% dose at 2 cm was computed from the measured dose. T.Plan refers to the dose at 2 cm according to the treatment plan. A 2% uncertainty was assigned to the calculation of the treatment plan dose. The last column compares the determined dose at 2 cm to the dose according to the treatment plan.

3.3 Exit dose

To verify the feasibility of using TLD for exit dose measurements, the following experiment was performed. The relative exit dose was measured with a parallel plate ionisation chamber and compared to TLD measurements. The phantom was made up of nylon 6 slabs with a total water equivalent thickness of 15.5 cm. The parallel plane ionisation chamber was positioned at a depth of 2 cm and the phantom was irradiated with a 0.5 Gy neutron dose. The parallel plate ionisation chamber was then positioned at the back surface of the phantom and again the phantom was irradiated with 0.5 Gy. In a third run, the TLDs were positioned at 2 cm and at the exit side of the phantom. The phantom was again irradiated with 0.5 Gy. The ratio of the dose measured at 2 cm to that at 15.5 cm was 0.55 ± 0.005 for the parallel plate ionisation chamber and 0.55 ± 0.012 for TLDs. The results agree within the experimental uncertainties.

Six of the nine fields that were subject to entrance in-vivo measurements were also used for simultaneous exit in-vivo dosimetry measurements. At the exit side of the patient the detectors were pasted on to the skin surface on the central axis of the beam exit. The measured exit dose was compared to the exit dose according to the treatment plan.

The exit dose is not routinely calculated in the treatment plan. To compare our exit dose measurements to the calculated exit dose the following procedure was employed. Each field of interest was separately calculated in the planning system. The isodose line at the field exit side was calculated and the exit dose was computed relative to the 100 % dose at 2 cm depth.

The treatment plan assumes full backscatter at the exit side of the patient, which in reality is not there. In order to compare the measured dose and the dose according to the treatment plan, we need to subtract the backscatter component in the treatment plan dose. Awschalom *et al.* (1982) investigated the effect of missing backscatter on the dose distribution of a p(66)Be(49) neutron beam at the Fermilab neutron therapy facility. The expression derived by Awschalom *et al.*(1982) is $D(t) = 1 - Ae^{-t/B}$, where D(t) is the normalized ionisation for backscattering thickness t, and A and B are a function of field size, A and B are $0.0165 + 0.0030EQS$ and $2.55 + 0.070EQS$ respectively. Results indicate that the dose reduction at the exit surface of the phantom due to the missing back scatter can be as large as 4% to 10% depending on the equivalent square field size. Since the neutron therapy facility at NAC is similar to the Fermilab facility, the results obtained at Fermilab are used for the backscatter correction in the NAC beam. The backscatter component was computed for each equivalent square field and subtracted from the treatment plan dose. Table 3.3 summarises the results.

Discrepancies up to -7.3 % were detected. A systematic discrepancy of – 5.1 % is apparent. The treatment plan does not correct for any patient inhomogeneity and is based on the assumption that the whole patient is water. These inaccuracies seem to lead to a systematic overestimation of the patient exit dose.

Patient information				Measured	Treatment plan				
Patients	Field no.	EQS [cm x cm]	Thickness [cm]	Exit dose [Gy]	100% [Gy]	% exit [%]	BSF [%]	Exit dose [Gy]	TLD /T.Plan
Patient 1	1	10.9	17	0.582 ± 0.012	1.226 ± 0.025	52	-4.92	0.606 ± 0.012	0.960 ± 0.029
	2	10.9	17	0.564 ± 0.004	1.226 ± 0.025	52	-4.92	0.606 ± 0.012	0.930 ± 0.021
Patient 2	2	8.8	32	0.161 ± 0.002	0.955 ± 0.019	19	-4.29	0.174 ± 0.003	0.925 ± 0.025
Patient 3	2	6.7	17.5	0.470 ± 0.009	1.189 ± 0.024	44	-3.66	0.504 ± 0.010	0.933 ± 0.028
Patient 4	2	7.5	15	0.432 ± 0.013	1.035 ± 0.021	45	-3.90	0.448 ± 0.009	0.964 ± 0.037
Patient 5	3	8.2	15	0.520 ± 0.007	1.126 ± 0.023	50	-4.11	0.540 ± 0.011	0.964 ± 0.024
Patient 6	4	10.5	20.2	0.167 ± 0.005	0.466 ± 0.009	39	-4.80	0.173 ± 0.003	0.965 ± 0.034

Table 3. 3: Exit dose measurements. 'Measured' refers to the dose measured at the exit patient skin surface with TLDs; 100 % is the dose at 2 cm depth according to the treatment plan. '% exit' refers to the percentage exit dose according to the treatment plan. BSF is the backscatter factor for each EQS calculated using Awschalom's expression. The exit dose is the dose according to the treatment plan minus the backscatter component. The last column is the ratio of the measured exit dose to the back scatter component corrected treatment plan dose.

Chapter 4: Glow curve analysis

4.1 Introduction

The TLD-700 glow curve exhibits a dominant peak (5) at about 250 ^{0}C and a second high temperature peak (6) at about 330 ^{0}C. Both have different absolute sensitivities and LET dependent sensitivities (Hoffmann *et al.*, 1983). The peak 6/5 ratio is therefore LET dependent and increases with increasing LET.

While glow curve analysis has been used to investigate the gamma component in neutron therapy beams (Meissner *et al.*, 1988), other authors have used the two-peak or high temperature method to determine the average LET of mixed radiation fields in space and in high altitude aircrafts (e.g. Noll *et al.*, 1996 and Vana *et al.*, 1996). We have investigated the peak 6/5 ratio in our neutron therapy beam with the aim of extracting further useful information from the glow curve and to relate changes in peak 6/5 ratio to changes in LET. We will investigate the behaviour of the peak 6/5 ratio in our p(66)/Be neutron therapy beam as a function of depth and off axis-distance.

4.2 Peak separation

The Solaro TLD software that is used to analyse glow curves does not allow the automatic separate analysis of peak 5 and 6. The peak 5 and 6 counts are obtained by manually analysing the glow-curve. Three methods of glow peak separation were evaluated. Firstly, peak 5 and peak 6 were separated by dividing the thermoluminescent integration time into two regions. Counts integrated between 160 ^{0}C and 300 ^{0}C are assigned to peak 5 while counts above 300 ^{0}C are assigned to peak 6. This method is referred to as manual integration. Secondly, the peak height was chosen as a measure of peak intensity. Lastly, both peaks were fitted using a curve fitting routine and counts were integrated accordingly. Figure 4.1 illustrates the last method. All three methods were applied to 10 glow curves of chips that had been irradiated in the neutron beam at various depths. Table 4.1 gives the peak height ratio as determined by the first two methods relative to the curve fitting method.

Peak 6/5 (curve fitting)	Manual curve fitting	Peak height curve fitting
0.132	1.57	0.93
0.129	1.56	0.96
0.104	1.52	0.88
0.093	1.51	0.81
0.076	1.48	0.86
0.075	1.55	0.87
0.074	1.61	0.81
0.079	1.58	0.82

Table 4. 1: Column 1 is the peak 6/5 ratio as determined by the curve fitting method. Column 2 and 3 give the peak 6/5 ratio determined by the manual integration and peak height methods relative to the peak 6/5 ratio determined by the curve fitting method.

The curve fitting procedure is very time consuming and the manual integration method was therefore used throughout the thesis. Since variation in peak 6/5 ratio rather than absolute peak 6/5 ratios were investigated, the error incurred by using manual integration was deemed acceptable. However, for future glow curve analysis, the peak height method is recommended.

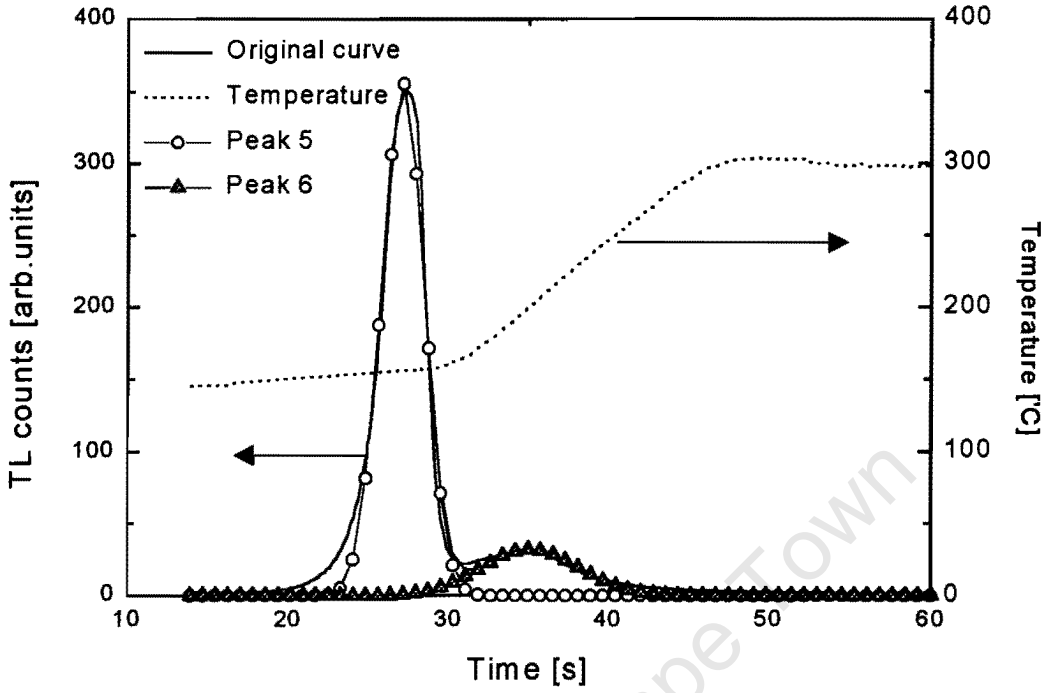

Figure 4. 1: Peak 5 and 6 analysed by a fitting program.

4.3 Dose linearity studies in neutron beam

The supralinear dose response of TLD-700 peak 6 has been observed in cobalt-60 beams but not in a d(14) + Be neutron beam (Pradhan *et al.*,1985, Rassow *et al.*, 1988). No linearity studies have been published for fast p(66)/Be neutron beams. Rassow *et al.* (1988) reported that the phenomenon of TLD peak dose supralinearity is a function of the beam's LET. Since the average LET of a p(66)/Be beams differs from that of a d(14)/Be beam (Pihet *et al.*, 1988), we investigated the peak 6 supralinearity in our beam.

All data is obtained from the experiment performed in section 2.4. The chip individual calibration factors determined in peak 5 were also used for peak 6. The dose response of peak 6 is shown in figure 4.2. The observed supralinearity makes the peak 6/5 ratio dose dependent. This effect needs to be corrected for before the peak 6/5 ratio dependency on LET can be investigated. In section 2.4, we have detailed the saturation correction of peak 5. The same formalism can be used to correct the supralinearity of peak 6. A curve fitting routine was applied to determine the absorbed dose as a function of thermoluminescent response. The following fourth order polynomial was derived and was later used to correct the dose non-linearity in subsequent measurements.

Absorbed dose (Gy) $= ar^3 + br^2 + cr + d$,

where a = 1.115, b = -2.6421, c = 3.9537, d = 0.0024 and r is a thermoluminescence response.

The equation was derived by reversing the axes and expressing the absorbed dose as a function of response. Since both equations (for peak 5 and 6) correct the non-linear TLD response in terms of given dose, the peak 6/5 ratio is unity by definition at the depth in the neutron beam where the dose linearity studies were performed.

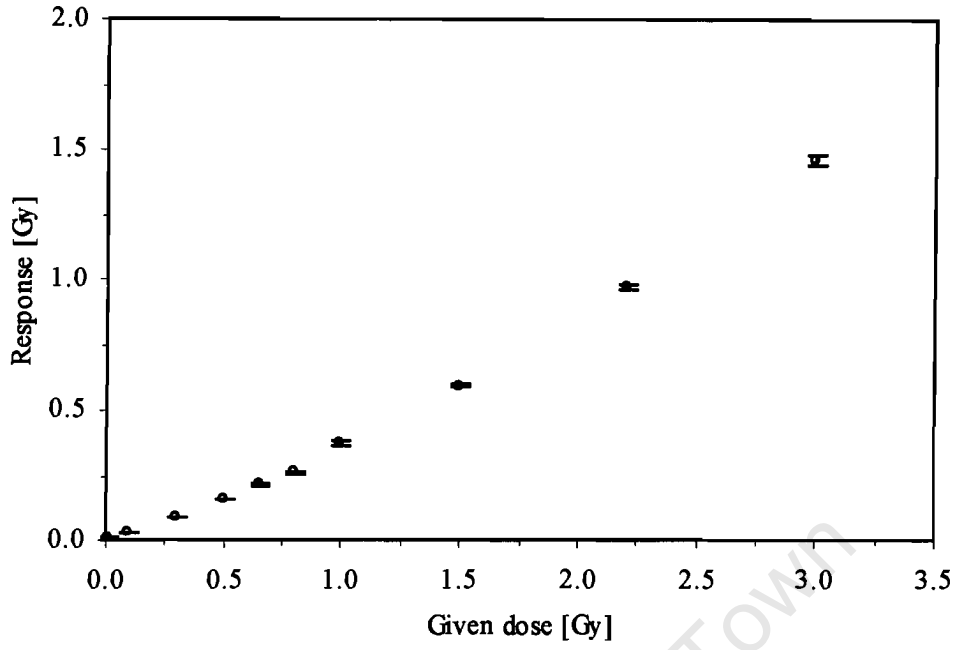

Figure 4. 2: Dose response of peak 6 of TLD-700.

4.4 Peak 6/5 ratio versus depth measurements

The neutron spectrum changes with depth due to beam hardening (Slabbert *et al.*, 1989, Hornsey *et al.*, 1988)). In chapter 2, the influence of this effect on the TLD sensitivity was investigated. In this chapter, we will investigate the influence of this effect on the peak 6/5 ratio. Results were obtained by analysing the peak 6/5 ratio of the TLD chips that were irradiated in the experiment described in section 2.4. Additional irradiations were done to investigate the peak 6/5 ratio in the built up region of the beam.

The peak 6/5 ratio was obtained by dividing the dose in peak 6 to the dose in peak 5. The results for a 5.5 cm x 5.5 cm field to 15 cm x 15 cm are shown in figure 4.3 to figure 4.6. The peak 6/5 ratio measured in all curves is relatively high at the surface and is fairly constant for deeper depths.

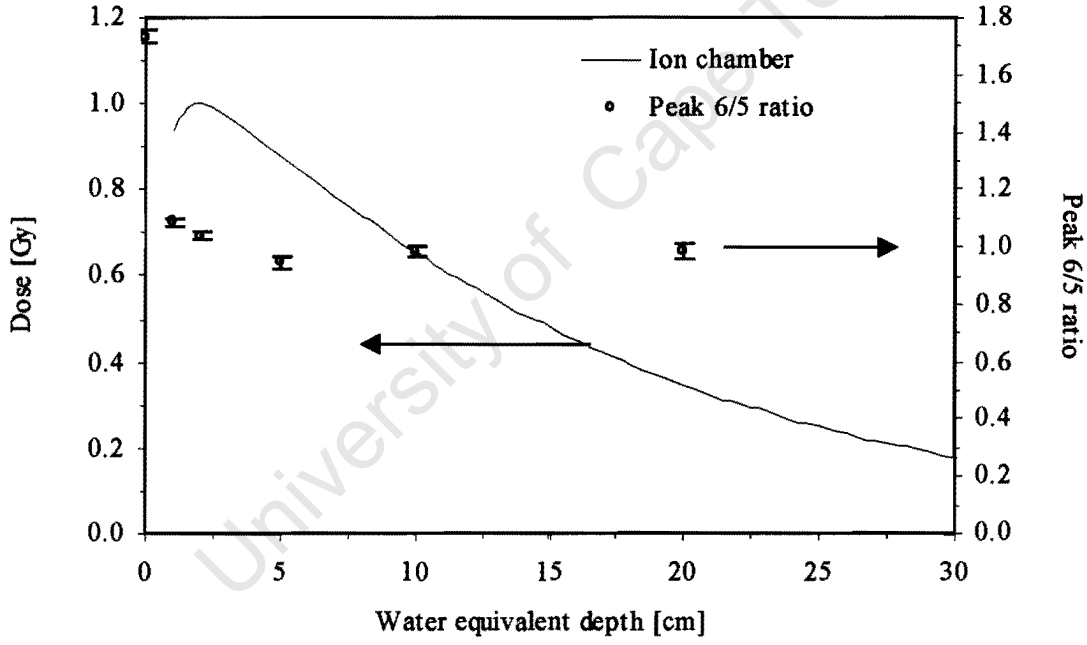

Figure 4. 3: Peak 6/5 ratio for a 5.5 x 5.5 cm field

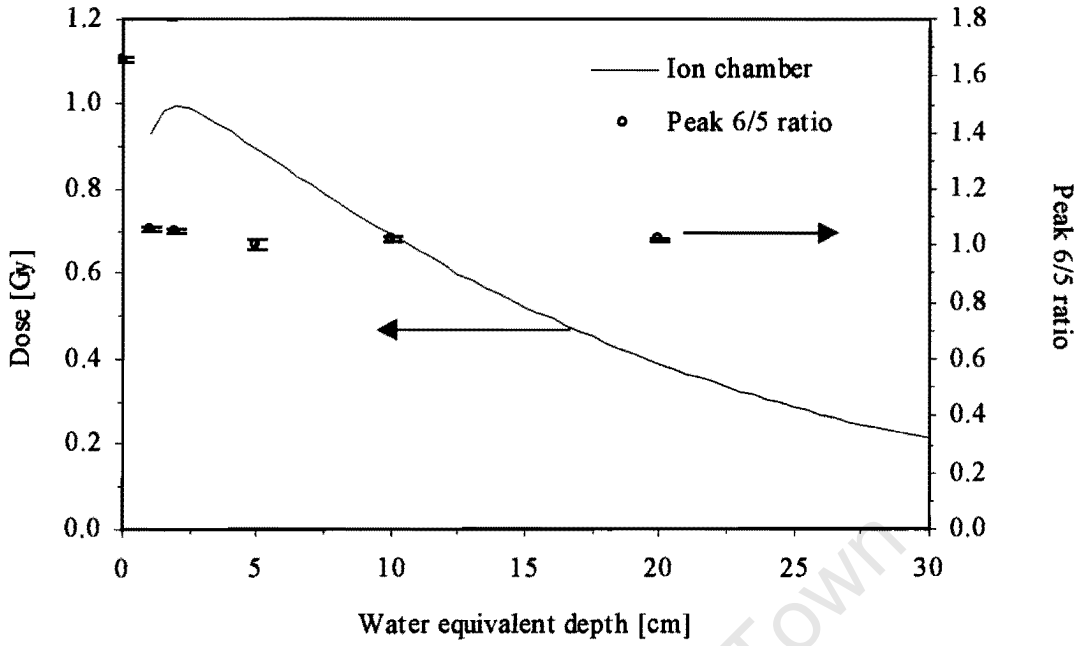

Figure 4. 4: Peak 6/5 ratio for a 8 cm x 8 cm field

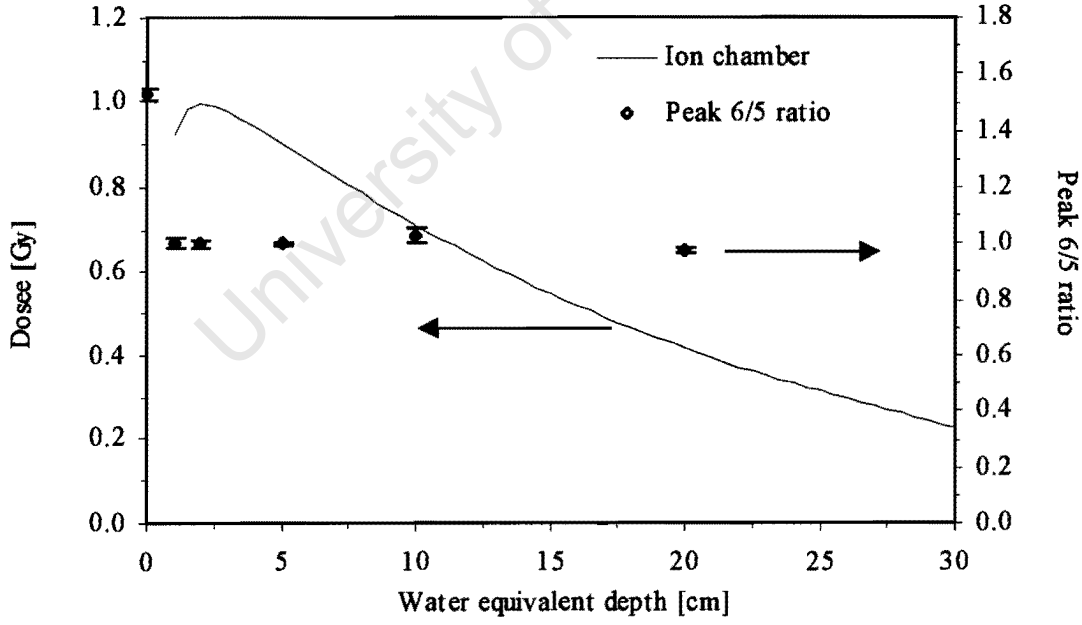

Figure 4. 5: Peak 6/5 ratio for a 10 cm x 10 cm field

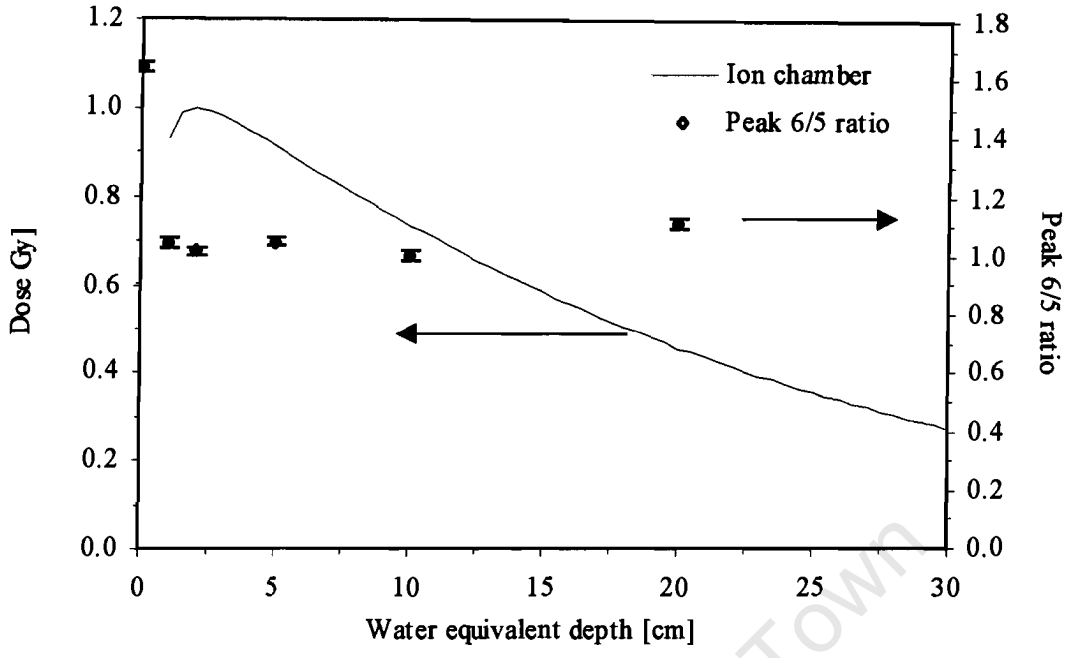

Figure 4. 6: Peak 6/5 ratio for a 15 cm x 15 cm field.

Investigations into the peak height ratio of TLD-700 dosimeters by Loncol *et al.* (1996) in a p(65)/Be beam showed that there was little change in the ratio with depth under comparable irradiation conditions, i.e. open beam and at depths ranging from 2 to 15 cm. The findings are in agreement with ours. This indicates that peak 6/5 ratio is not sensitive to the beam quality changes observed in the NAC beam at depth by Slabbert *et al.* (1989) and Binns *et al.*, 1992. However, the observed high peak 6/5 ratio at the surface prompted an investigation of the peak 6/5 ratio in the built up region.

A nylon phantom and sheets of 1 mm A150 build up were used in the experiment. In the first set-up, 8 TLDs were placed at the surface of the phantom without build up and were irradiated. This procedure was then repeated in steps of 1 mm until a depth of 20 mm was attained, i.e. 1 mm of A150 build up was added each time. Each set up was irradiated with a dose of one gray defined at 2 cm depth. The results are shown in figure 4.7. The extrapolation chamber measurements were plotted for comparison (Jones *et al.*, 1994).

The neutron beam produces secondary charged particles that have different ranges in tissue and attain equilibrium at different depths. The alpha particles and heavy nuclei have short ranges in tissue and attain equilibrium at shallower depths. The low LET, recoil protons attain equilibrium at a depth of 16 mm (Binns, 1993). In the build up region, the average LET of the secondary charged particles decreases with depth. Once the charged particle equilibrium is established, the peak 6/5 ratio remains constant. Hence the peak 6/5 ratio qualitatively follows the expected decrease in LET in the built up region (Binns, 1993).

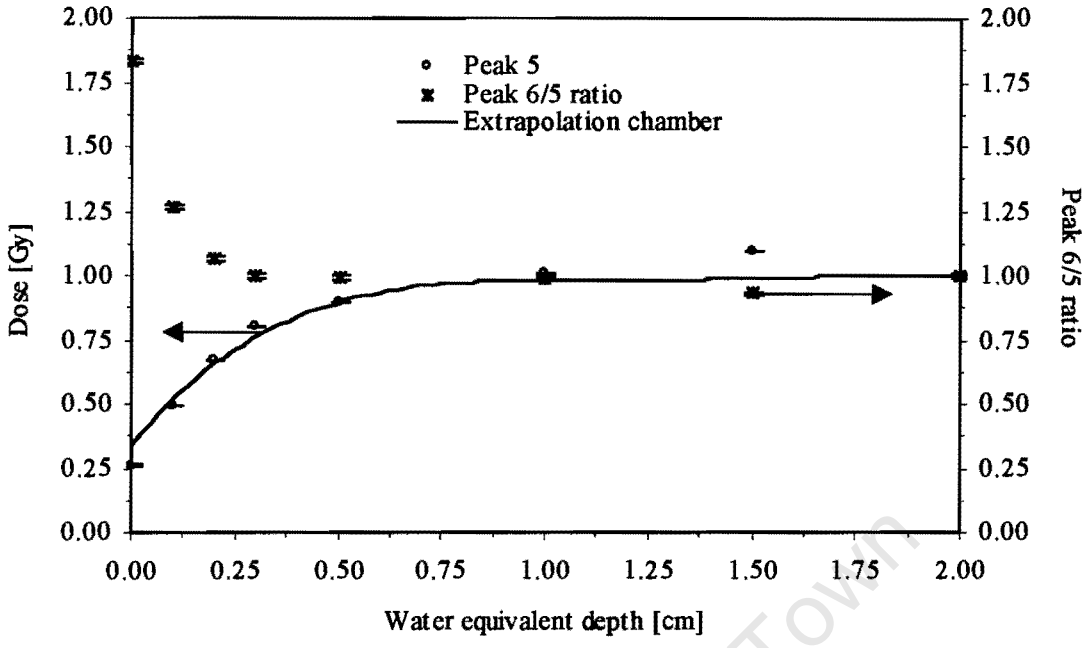

Figure 4. 7: Peak 6/5 ratio as a function of depth in the build up region. Extrapolation chamber measurements are also plotted.

4.5 Peak 6/5 ratio in beam profile measurements

The softening of the neutron beam as a result of beam scattering and the sharp increased in the photon component both affect the quality of the therapy beam in the penumbra region. In the following experiments, we aim to determine the changes in the peak 6/5 ratio with off-axis distance.

In the first experiment, the TLD chips were irradiated in a 5.5 cm x 5.5 cm field in the central axis of the beam and at distances of 1 – 5 cm off-axis. The peak 6/5

ratio as a function of off-axis distance is shown in figure 4.8. The peak 6/5 ratio is fairly constant within the irradiation field and seems to increase with off-axis distance. To extend this study to a wider off-axis distances, chips were irradiated in a second experiment each at distances up to 9 cm off-axis. Four chips were irradiated at each off-axis distance. The peak 6/5 ratio remains constant within the direct radiation field and increases up to a distance of 9 cm off-axis (figure 4.9).

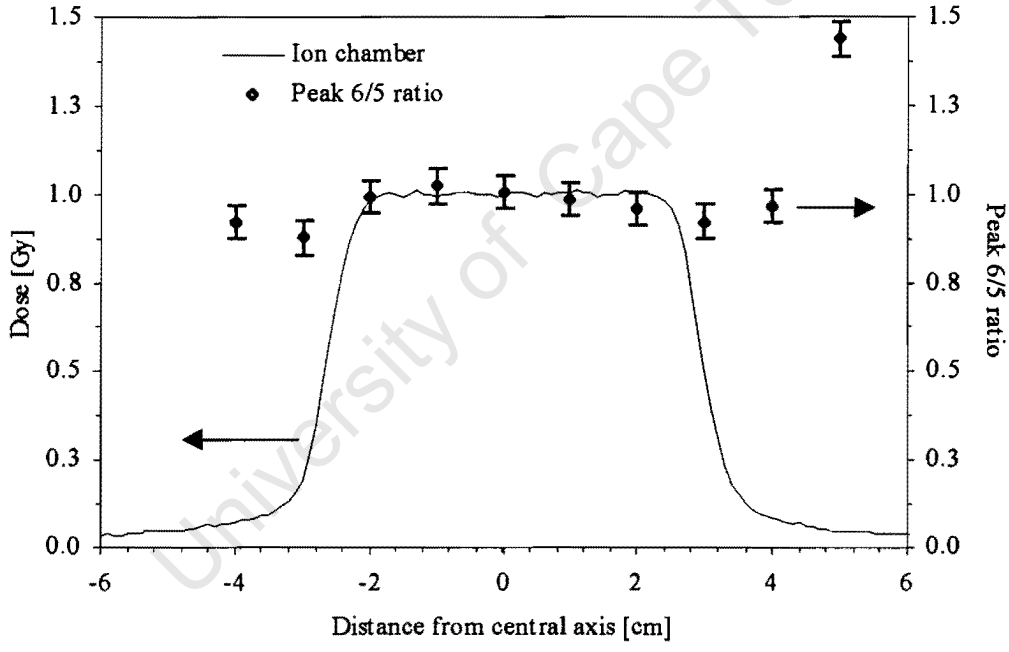

Figure 4. 8: Peak 6/5 ratio versus off-axis distance for a 5.5 cm x 5.5 cm field.

In the penumbra region the gamma components rises sharply (Jones *et al.*, 1995 and Binns, 1993). This effect lowers the peak 6/5 ratio since the peak 6/5 ratio

measured in a cobalt-60 beam is smaller than in a neutron, i.e. high LET, beam. However, the neutron component in the penumbra region consists of scattered lower energy neutrons that possess a higher average LET which increases the peak 6/5 ratio in this region. Hence, in the penumbra region two physical processes occur of which one lowers the peak 6/5 ratio whereas the other increases the peak 6/5 ratio. A rise in the peak 6/5 ratio is observed in the penumbra region which indicates that the change in the neutron component's composition is the dominating effect in terms of the peak 6/5 ratio.

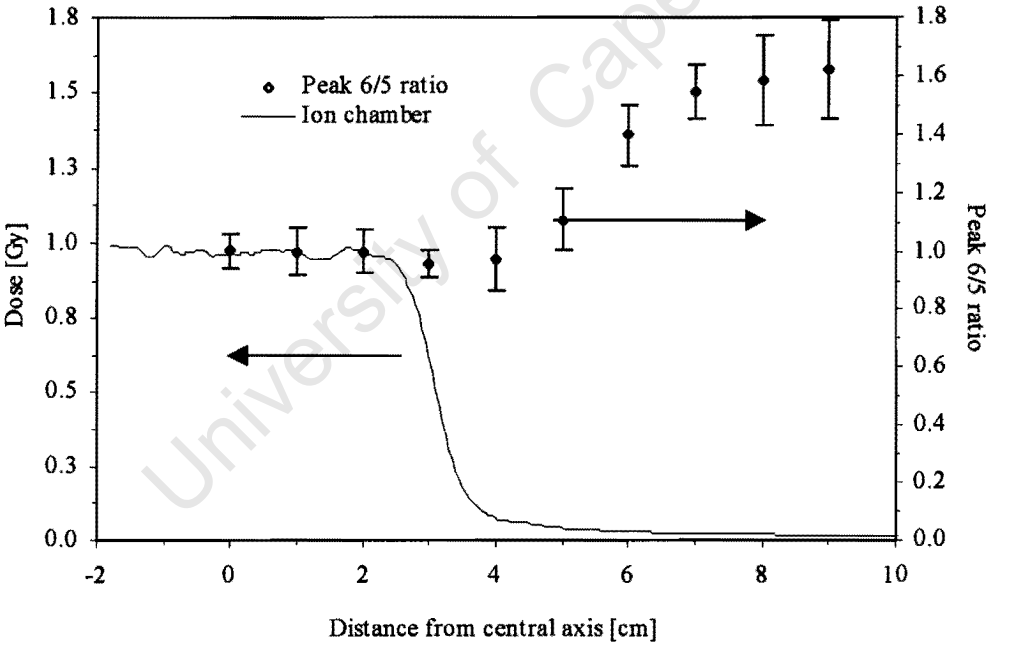

Figure 4. 9: Peak 6/5 ratio outside beam axis.

The peak 6/5 ratio in the penumbra region can be divided into a neutron and gamma component; $\left(\frac{p6}{p5}\right)_{comb.} = \left(\frac{p6}{p5}\right)_n . n_c + \left(\frac{p6}{p5}\right)_\gamma . \gamma_c$,

where $\left(\frac{p6}{p5}\right)_{comb}$ is the combined, i.e. measured peak 6/5 ratio, $\left(\frac{p6}{p5}\right)_n$ and $\left(\frac{p6}{p5}\right)_\gamma$ are the peak 6/5 ratios due to the neutron and gamma components, and n_c and γ_c are the neutron and gamma components respectively. The gamma component has been measured in the penumbra region (Jones *et al.*, 1995 and Binns, 1993), which allows the determination of n_c and γ_c as a function of off-axis distance. The $\left(\frac{p6}{p5}\right)_\gamma$ value can be determined from TLD-700 irradiations in a cobalt-60 beam. This allows the calculation of the $\left(\frac{p6}{p5}\right)_n$ ratio as a function of off-axis distance. Figure 4.10 shows the results of this evaluation. Accompanying microdosimetry measurements would allow the determination of $\left(\frac{p6}{p5}\right)_n$ ratio as a function of the dose averaged lineal energy $\bar{y}_D$ ($\bar{y}_D$ is explained in section 1.5).

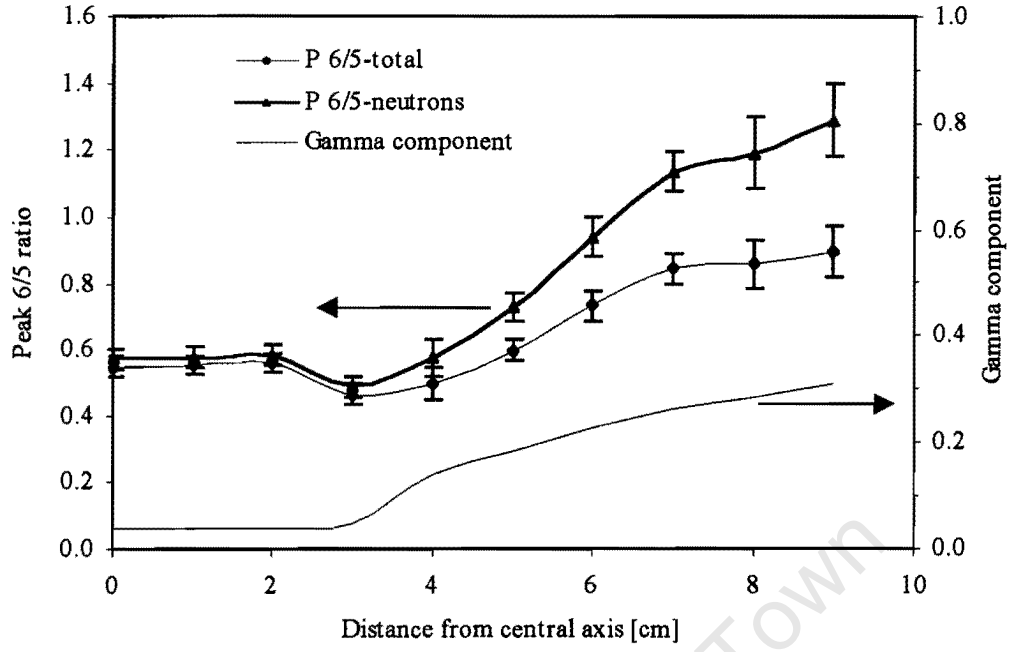

*Figure 4. 10: The variation of peak 6/5 ratio with off-axis distance. The gamma component (*Jones *et al.*, 1992*) is also plotted against off-axis distance.*

The peak 6/5 ratio measurements follow the expected increase in the average LET in the penumbra region. These measurements in combination with those done in the built up region allow the conclusion that the peak 6/5 ratio as measured with TLD-700 gives an indication of the relative beam quality.

Chapter 5: Summary and conclusion

In this project, TLD-700 chips have been employed for absorbed dose measurements in a p(66)/Be therapeutic neutron beam. After careful chip selection, the detectors were calibrated in the neutron beam and the chip specific calibration factors were determined, which were used in all subsequent measurements.

The dose non-linearity was determined in the dose ranging from 1 Gy to 3 Gy in the p(66)/Be neutron beam. Saturation was observed in peak 5 and supralinearity was observed in peak 6. The dose non-linearity correction equations were derived for peak 5 and peak 6 separately and were used to correct the dose non-linearity in subsequent measurements. The TLD sensitivity at depth in the phantom was determined by irradiating TLD chips at different depths in the phantom. The peak 5 sensitivity was found to be constant with depth. Measurements of the beam profile were performed. Changes in the TLD sensitivity relative to ionisation chamber measurements were observed in the penumbra region where the beam quality changes.

Actual in-vivo dose measurements were performed in the direct neutron field after characterising the TLD chips in the phantom. In-vivo measurements were performed on seven patients (9 fields). Entrance in-vivo dose measurements were measured under 2 mm thick A150 tissue equivalent plastic built up. The patient entrance doses determined with TLDs are in good agreement with the treatment plan doses (Table 3.2). Maximal deviations of 3.2 % were detected and a systematic difference of 1.7 % exists between the TLD measurements and the treatment plan doses. Exit doses were measured on six patients (7 fields). Discrepancies up to –7.3 % were detected on the exit side and a systematic difference of –5.1 % was apparent between the TLD measurements and the treatment plan exit doses (Table 3.3).

The glow peak 6 over 5 ratio was determined in our beam with the aim of extracting further useful information from the TLD glow curve. This ratio was found to be high at the surface of the phantom, it decreases in the built up region remains constant with depth thereafter. The peak 6/5 ratio was found to increase with off axis distance. The peak 6/5 ratio changes in areas where qualitative changes in the therapy beam occur and can be used as an indication of the relative beam quality.

In conclusion, we demonstrated the feasibility of using TLD-700 chips as an in-vivo dosimeter in fast neutron therapy beams for entrance and exit dose

measurements. These detectors can also be useful to determine relative changes in the beam quality.

References

- Alex R, Alecu M (1999). In-vivo rectal dose measurements with diodes to avoid misadministration during intracavitary high dose rate brachytherapy for carcinoma of the cervix, *Med. Phys.* **26(5),** 768 - 770.
- Amor Duch M, Ginjaume M (1998). Thermoluminescent dosimetry applied to in vivo dose measurements for total body irradiation technique, *Radiother. Oncol.* **47,** 319 – 324.
- Angelone M, Yudelev M, Kota C, Maughan RL (1998). Measurement of the neutron sensitivity of TLD-300 irradiated in tissue equivalent phantom by d(48.5) + Be neutrons, *Med. Phys.* **25(4),** 512 – 515.
- Awschalom M, Rosenberg I (1980). Characteristics of a p(66)Be(49) neutron therapy beam II: Skin sparing and dose transition effects, *Med. Phys.* **8(1),** 105 – 107.
- Awschalom M, Rosenberg I, Mravca A (1983). Kermas for various substances averaged over the energy spectra of fast neutron therapy beams: A study of uncertainties, *Med. Phys.* **10(4),** 395 – 409.
- Awschalom M, Rosenberg I, Ten Haken RK (1982). The effect of missing backscatter on the dose distribution of a p(66)Be(49) neutron therapy beam, *Med. Phys.* **9(4),** 559 – 562.
- Bewley DK. (1989). The Physics and Radiobiology of fast neutron beams, Adam Hilger, Bristol and New York.
- Binns PJ, Hough JH (1988). Lineal energy measurements in two fast neutron beams: d(16) + Be and p(66) + Be, *Radiat. Prot. Dosim.* **23(1-4),** 358 – 388.
- Binns PJ, Hough JH. (1992). Consideration of radiation quality in treatment planning with p(66)/Be(40) neutrons, *Int. J. Radiat. Oncol. Biol. Phys.* **24,** 975 – 981.
- Binns PJ. (1993). Microdosimetry for a fast neutron beam, PhD Thesis, University of Cape Town.

- Blake SW, Bonnett DE, Finch J (1990). A comparison of two methods of in-vivo dosimetry for a high energy neutron beam, *Brit. J. Radiol.* **63,** 476 – 481.
- Blum E, Heather JD, Beal ADR, Bewley DK (1976). Calcium sulphate phosphor for clinical neutron dosimetry, *Health Phys.* **30,** 275 – 261.
- Cameron JR, Suntharalingam N, Kenny GN (1968). Thermoluminescent dosimetry, University of Wisconsin Press, Madison.
- Essers M, Mijnheer BJ. (1999). In vivo dosimetry during external photon beam radiotherapy, *Int. J. Radiat. Oncol. Biol. Phys.* **43(2),** 245 – 259.
- Field SB (1971). An in vivo dosimeter for fast neutrons, *Brit. J. Radiol.* **44,** 891 - 892.
- Goitein M (1983). Nonstandard deviations, *Med. Phys.* **10,** 709 – 711.
- Hall EJ (1988). Radiobiology for the radiologist, J.B. Lippincott Company, Philadelphia.
- Hall EJ, Zaider M, Bird R, Astor M (1982). Radiobiological studies with therapeutic neutron beams generated by p+ → Be or d+ → Be, *Brit. J Radiol.* **55,** 640 – 644.
- Hess A, Schmidt R, Thom M (1991). Dosimetric investigations in the dose build up using bolus techniques for fast neutron therapy, *Med. Phys.* **18(4),** 829 – 831.
- Heukelom S, Lanson JH, Miljnheer BJ (1991). Comparison of entrance and exit dose measurements using ionisation chambers and silicon diodes, *Phys. Med. Biol.* **36,** 47–59.
- Hocini B, Djeffal S, Vynckier S, Wambersie A (1988). Response of ^{7}LiF thermoluminescence dosimeters to clinical neutron beams with energies ranging from d(14) + Be to p(75) + Be, *Radiat. Prot. Dosim.* **23(1-4),** 417 – 419.
- Hoffmann W (1976). TL dosimetry in high LET radiotherapeutic fields, *Radiat. Prot. Dosim.* **66(1-4),** 243 – 248.

- Hoffmann W, Prediger B (1983). Heavy particle dosimetry with high temperature peaks of CaF_2: Tm and ^7LiF phosphors, *Radiat. Prot. Dosim*, **6(1-4)**, 149 – 152.
- Hornsey S, Myers R, Parnell CJ, Bonnet DE, Blake SW, Bewley DK (1988). Changes in relative biological effectiveness with depth of the Clatterbridge neutron therapy beam, *Brit. J. Radiol.* **61**, 1058 – 1062.
- ICRU 24 (1976). Determination of absorbed dose in a patient irradiated by beam of x and gamma rays in Radiotherapy Procedures, ICRU Report 24, Bethesda, MD.
- ICRU 36 (1983). Microdosimetry, ICRU Report 36, Bethesda, Maryland
- Jones DTL (2000), Private communication.
- Jones DTL, Yudelev M (1989). *NAC Annual Report*, **NAC/AR/89-01**, 142 – 166.
- Jones DTL, Schreuder AN, Symons JE (1992). *NAC Annual Report*, **NAC/AR/92-01**, 72 - 73.
- Jones DTL, Schreuder AN, Symons JE (1995). Particle Therapy at NAC: Physical Aspects, Proc. of 14th International Conference on Cyclotrons and their Applications, Cape Town, South Africa, 491 - 498.
- Jones DTL, Schreuder AN, Symons JE, Binns PJ (1997). Experimental investigation of a multiblade trimmer for neutron therapy, *J. of Brachytherapy Int'l.* **13**, 59 – 66.
- Jones DTL, Schreuder AN, Symons JE, de Kork EA, Vernimmen FJA, Stannard CE, Wilson J, Schmitt G (1999). Status report of the NAC Particle therapy program, *Strahlenther. Onkol.* **175(Supp 2)**, 30 – 32.
- Jones DTL, Schreuder AN, Symons JE, Yudelev M (1994). The NAC particle therapy facilities, *Hadrontherapy in Oncology*, Elsevier Science B.V, 307 – 328.
- Khan FM (1994). The Physics of radiation therapy, Williams & Wilkins, Baltimore.

- Kron T (1999). Application of thermoluminescence dosimetry in medicine, *Radiat. Prot. Dosim.* **85(1-4),** 333 – 340.
- Leunens G, Van Dam J, Dutreix A, van der Schueren E (1990). Quality assurance in radiotherapy by in vivo dosimetry. Entrance dose measurements, a reliable procedure, *Radiother. Oncol.* **17,** 141 – 151.
- Loncol T, Greffe JL, Vynckier S, Scalliet P (1996). Entrance and exit dose measurements with semiconductors and thermoluminescent dosimetors: a comparison of methods and in vivo results, *Radiather. Oncol.* **41,** 179 – 187.
- Loncol T, Vynckier S, Wambersie A (1996). Thermoluminescence in proton and fast neutron therapy beams, *Radiat. Prot. Dosim*, **66(1-4),** 299 – 304.
- McKinlay AF (1981). Thermoluminescence dosimetry, Adam Hilger Ltd, Bristol.
- Meissner P, Bienek U, Rassow J (1988). Application of TLD-700 detectors for dosimetry in d(14) + Be neutron fields, *Radiat. Prot. Dosim,* **23(1/4),** 421 – 424.
- Mijnheer BJ, Battermann JJ, Wambersie A (1987). What degree of accuracy is required and can be achieved in photon and neutron therapy, *Radiother. Oncol.* **8,** 237 – 252.
- Noll M, Schöner, Vana N, Fugger M, Egger E (1997). Measurements of the LET in a proton beam on 62 MeV using HTR-Method, Microdosimetry; An Interdisciplinary Approach, The Royal Society of Chemistry, Cambridge, 274 – 278.
- Noll M, Vana N, Schöner W, Fugger M (1996). Measurements of equivalent dose in aircraft with TLDs, *Radiat. Prot. Dosim.* **85(1-4),** 283 – 286.
- Page BC, Bewley DK (1984). The use of fast neutron dosimeter diodes for in-vivo dosimetry in neutron therapy, *5th Symposium on neutron dosimetry,* Munich, 1097 – 1106.

- Pihet P, Gueulette J, Menzel HG, Grillmaier RE, Wambersie A (1988). Use of microdosimetric data of clinical relevance in neutron therapy planning, *Radiat. Prot. Dosim.* **23(1-4)**, 471 – 474.
- Pradhan AS, Rassow J, Meissner P. (1985). Dosimetry of d(14) + Be neutrons with the two-peak method of LiF TLD-700, *Phys. Med. Biol.* **30(12),** 1349 – 1354.
- Raju MR (1996). Particle radiotherapy: Historical developments and current status, *Radiat. Res.* **145**, 391 – 407.
- Rassow J, Klein C, Meissner P (1988). Supralinearity behaviour of TLD-300 and TLD-700, *Radiat. Prot. Dosim,* **23(1-4),** 409 – 412.
- Rosenberg I, Awschalom M (1981). Characterization of a p(66)Be(49) neutron therapy beam 1: Central axis depth dose and off-axis ratios, *Med. Phys.* **8(1),** 99 – 104.
- Schöner W, Vana N, Fugger M (1999). The LET dependence of LiF:Mg,Ti dosimeters and its application for LET measurements in mixed radiation fields, *Radiat. Prot. Dosim,* **85(1-4),** 263 – 266.
- Slabbert JP, Binns PJ, Jones HL, Hough JH (1989). A quality assessment of the effects of a hydrogenous filter on a p(66) Be(40) neutron beam, *Brit. J. Radiol.* **62**, 989 – 994.
- Smith A, Shan GA, Kron T (1998). Variation of patient doses in head CT, *Brit. J. Radiol.* **71(852)**, 1296 - 1301.
- Smith RA, Rosen II, Hogstrom KR (1977). The silicon diodes as an in-vivo dosimeter for fast neutrons, *Int. J. Rad. Oncol. Biol. Phys.* **2**, 111 – 116.
- Stannard CE (1998). *NAC Annual Report.* 104 – 106.11.
- Stone (1948). Neutron therapy and specific ionization, *Am. J. Roentgenol. & Rad. Therapy,* **59,** 771 – 784.
- Vana N, Schöner W, Fugger M, Akatov Y (1996). Absorbed dose measurement and LET determination with TLDs in space, *Radiat. Prot. Dosim,* **66(2),** 145 – 150.

❖ Waligorski MPR, Katz R. (1980). Supralinearity of peak 5 and peak 6 in TLD-700, *Nucl. Inst. Meth.* **172**, 463 – 470.

❖ Wambersie A (1992). Neutron therapy: From radiobiology expectation to clinical reality, *Radiat. Prot. Dosim.* **44 (1-4),** 379-395.

❖ Wambersie A, Auberger T, Gahbauer R, Jones DTL, Potter R (1999). A challenge for high precision radiation therapy: The case for hadrons, *Strahlenther. Onkol.* **175 Suppl 2,** 122 – 128.